ELSEVIER

International Journal of Solids and Structures 41 (2004) 2581–2606

INTERNATIONAL JOURNAL OF SOLIDS and STRUCTURES

www.elsevier.com/locate/ijsolstr

Effect of T-stress on fatigue crack closure in 3-D small-scale yielding

S. Roychowdhury, R.H. Dodds Jr. *

Department of Civil and Environmental Engineering, 2129 Newmark Laboratory, University of Illinois, 205 N. Mathews Avenue, Urbana, IL 61801, USA

Received 9 April 2003

Abstract

This paper investigates the effects of in-plane constraint on 3-D fatigue crack closure in the small-scale yielding regime. The finite element analyses grow a sharp, straight-through crack in a modified boundary layer model under mode I, constant amplitude cyclic loading with prescribed but independent peak values of stress intensity factor, K_{max}, and the T-stress, T_{max}. A purely kinematic hardening law with constant modulus represents the material constitutive behavior. The computational results demonstrate that a two parameter characterization of crack tip fields in terms of $K_{max}/\sigma_0\sqrt{B}$ and T_{max}/σ_0, where σ_0 denotes the yield stress of the material, correlates successfully the normalized opening load K_{op}/K_{max} across variations of thickness (B), constraint level and material flow properties. Both negative and positive T-stress reduce the through-thickness variation in local opening load levels along the crack front. A negative T-stress increases K_{op}/K_{max} values, particularly at low peak loads where the plastic zone size remains a fraction of the thickness; a positive T-stress has limited effect on K_{op}/K_{max} values. The fringe plots of individual plastic strain components reveal (a) in the absence of T-stress ($T_{max}/\sigma_0 = 0$), plastic contraction in the thickness direction compensates primarily for permanent stretching in the direction normal to the crack plane required for closure, (b) for negative T-stress ($T_{max}/\sigma_0 < 0$), plastic contraction in the in-plane transverse direction contributes the larger share of material flowing into the normal direction, and (c) for positive T-stress ($T_{max}/\sigma_0 > 0$), both in-plane directions experience permanent stretching and the thickness direction alone undergoes plastic contraction.
© 2003 Elsevier Ltd. All rights reserved.

Keywords: Fatigue; Crack closure; In-plane constraints; T-stress; Opening load; Plastic flow; Small-scale yielding; 3-D finite element analysis

1. Introduction

Premature closure of crack surfaces influences greatly the rates of fatigue crack growth (Suresh, 1991). To account for crack closure, design procedures routinely employ a modified Paris-law type relationship of the form

* Corresponding author. Tel.: +1-217-333-3276; fax: +1-217-333-9464.
E-mail address: rdodds@uiuc.edu (R.H. Dodds Jr.).

0020-7683/$ - see front matter © 2003 Elsevier Ltd. All rights reserved.
doi:10.1016/j.ijsolstr.2003.11.004

$$\frac{da}{dN} = C(\Delta K_{\text{eff}})^m, \tag{1}$$

where the LHS represents the instantaneous crack growth per cycle, and C and m are material properties. The effective range of the stress intensity factor, $\Delta K_{\text{eff}} = K_{\max} - K_{\text{op}}$, quantifies the crack driving force where $K_{\max}$ denotes the maximum stress intensity factor (K_{I}) in a load cycle computed as a through-thickness average value remote from the crack front, and K_{op} represents the value of K_{I} when the crack first opens completely during the load cycle. In metallic materials, directional plastic flow in the region around crack front constitutes a primary mechanism enabling crack closure at load levels above threshold. Specimen geometry, material properties, deformation pattern (plane stress or plane strain), etc. all influence the near-tip plastic deformation. Numerical investigations of such plasticity induced crack closure (PICC) in fatigue crack growth seek to determine the effects of these variables on the crack driving force, ΔK_{eff}.

The majority of numerical studies to date employ two-dimensional (2-D) models (McClung, 1999) which neglect through-thickness variations of the closure process. The 2-D models provide a restricted framework to investigate the effect of thickness constraint through only the limiting cases of plane strain and plane stress. In real structures and specimens, deformations evolve in more complex patterns than the ones envisaged in these limiting cases. To study the effects of thickness and material flow properties on PICC, Roychowdhury and Dodds (2003a) simulate fatigue crack growth under 3-D small-scale yielding (SSY) conditions using a boundary layer representation. Such conditions represent thin metallic components and test specimens subjected to moderate-to-high cycle fatigue loading. The peak load, $K_{\max}$, remains a small fraction of the fracture toughness, K_c, and consequently produces plastic zones comparable in size to thickness B and much smaller than any in-plane characteristic dimensions (e.g. the crack length, the remaining ligament, distance to a nearby boundary or load application point, etc.).

For SSY configurations, Roychowdhury and Dodds (2003a) demonstrate the existence of a *similarity scaling relationship* that couples in a unique way the effective stress intensity factor, $\Delta K_{\text{eff}} = K_{\max} - K_{\text{op}}$, to the peak load in each cycle, the specimen thickness and the material flow properties. In particular, we show through numerical computations that for fatigue loading at a constant $K_{\min}/K_{\max} = R = 0$ and zero T-stress, the $K_{\text{op}}/K_{\max}$ value at each location along the crack front remains unchanged when $K_{\max}$, thickness (B) and material flow stress (σ_0) all vary to maintain a fixed value of $\overline{K} = K_{\max}/\sigma_0\sqrt{B}$. A subsequent paper by Roychowdhury and Dodds (2003b) demonstrates the validity of the similarity scaling relationship for $R = 0.1$ loading (a value commonly adopted in experimental programs) and emphasizes the role of the quantity $\overline{K} = K_{\max}/\sigma_0\sqrt{B}$ as a non-dimensional scaling measure for fatigue loading. Under SSY conditions, the plastic zone ahead of the crack grows in proportion to the quantity $(K_{\text{I}}/\sigma_0)^2$. Thus, the parameter $\overline{K}$ essentially describes the in-plane plastic zone size at the peak of the load cycle relative to the thickness.

Developments of $\overline{K}$ scaling to date have focused on zero T-stress loading—a condition found, for example, in SE(B) specimens with $a/W \approx 0.39$ as well as a few other selected geometries (Sherry et al., 1995). The T-stress is a non-singular, constant stress quantity parallel to the direction of crack extension under mode I loading (Williams, 1957) (see also Section 3). Under SSY conditions, the T-stress approximates the effects of in-plane geometry and loading (e.g. tension vs. bending) on plastic deformation around the crack tip and on the fracture process (Larsson and Carlsson, 1973; Rice, 1974; Betegon and Hancock, 1991; Du and Hancock, 1991; Wang and Parks, 1992; Xia and Shih, 1995; Ruggieri and Dodds, 1996; Jayadevan et al., 2002).

The works of Hancock et al. (1991) and Hancock (1992) first validated the T-stress as an appropriate parameter to characterize crack-tip constraint in a wide range of configurations. These studies also demonstrate that geometries associated with negative T-stress exhibit an enhanced initiation toughness and resistance to ductile crack growth. In contrast, positive T-stress configurations exhibit (nearly) geometry-independent toughness. The linear-elastic perturbation analyses by Cotterell and Rice (1980) show that the

crack path can become unstable for positive T-stress geometries. Thus, T-stress plays an important role in the fracture behavior of many engineering structures.

This paper examines the influence of in-plane constraint variations imposed through T-stress on plasticity driven fatigue crack closure. Initial results confirm the existence of the $\overline{K}$ scaling relationship at different constraint levels encountered in structures. The computational results demonstrate that in 3-D SSY, a two parameter characterization of crack-tip fields in terms of $K_{\max}/\sigma_0\sqrt{B}$ and $T_{\max}/\sigma_0$ correlates successfully the normalized opening load $K_{\mathrm{op}}/K_{\max}$ across variations of thickness, specimen geometry (approximated through the T-stress) and material flow properties. Here, $T_{\max}$ denotes the maximum value of the T-stress reached in the loading cycle. The focus then turns to investigate the effect of T-stress on the opening load, K_{op}, and reveals the strong roles played by the T-stress on crack closure. The analyses consider two magnitudes of non-dimensional loading $\overline{K}$. For the smaller value, the maximum plastic zone size directly ahead of the crack tip extends a fraction ($\sim$20%) of the thickness. For the larger value, plastic deformation extends a distance on the order of the thickness. Crack surface profiles and strain fringe plots reveal features of the three-dimensional (3-D) plastic flow leading to closure under various levels of T-stress.

The plan of the paper is as follows: Section 2 reviews prior numerical studies that address the influence of in-plane constraint on the fatigue crack closure. Section 3 describes details of the modified 3-D SSY model for crack closure analysis. Section 4 outlines the finite element modeling and numerical procedures to construct the crack growth solutions. Section 5 presents and discusses key results of the study. Finally, Section 6 lists the main conclusions drawn from the present work.

2. Background

Fleck and Newman, FN (1988) study PICC under plane-strain conditions for an elastic-perfectly plastic material. They employ a 2-D finite element model to simulate fatigue crack growth in two different specimen geometries. At load ratio $R = 0$, they observe crack closure in a center-cracked panel, M(T), but not in a bend specimen, SE(B). FN rationalize the influence of specimen geometry on closure behavior in terms of the T-stress, which has negative values for the M(T) specimen and positive values for the SE(B) specimen. This explanation extends to fatigue loading the work of other researchers (Larsson and Carlsson, 1973; Rice, 1974) which show strong T-stress effects on the SSY response of stationary cracks. Specifically, the crack opening displacement and plastic zone size for stationary cracks are unique functions of K, T, and material flow properties for a range of geometries modeled in plane strain. The work by FN also confirms the intuitive understanding that crack-tip singularity elements should not be used in analyses of fatigue crack growth, since the nature of crack tip singularity for the fatigue crack differs from that of a stationary crack.

Fleck (1986) employs a similar computational model to study more closely the effects of T-stress in other 2-D idealizations. He concludes that under plane-strain conditions, PICC occurs only when the ratio $T_{\max}/\sigma_0$ remains less than an undetermined critical value in the range of 0.035–0.070. The normalized opening load $P_{\mathrm{op}}/P_{\max}$ increases with decreasing T-stress and reaches a value of $\sim$0.28 for $T_{\max}/\sigma_0 = -0.35$. However, under plane-stress conditions the normalized opening load remains independent of T-stress for the range of magnitudes considered ($-0.35 \leqslant T_{\max}/\sigma_0 \leqslant 0.07$).

Fleck (1986) also observes that closure in plane strain occurs during the very early stages of growth. The magnitude of $P_{\mathrm{op}}/P_{\max}$ rises as the crack tip passes through the initial plastic zone created by the first excursion to peak load and then decays to zero. A residual wedge of material left near the initial crack tip leads to a subsequent "discontinuous" closure profile (some small regions behind the current crack tip do not close). Under plane-stress conditions, the crack always opens and closes in a continuous manner. These observations contrast the continuous "zipping" and "unzipping" of crack surfaces noted by McClung et al. (1991) for both plane strain and plane stress. Our previous work (Roychowdhury and Dodds, 2003b) shows

that in a 3-D configuration, the crack opens in a continuous manner at the (outside) free surfaces. The mid-plane exhibits little or no closure at low load ($\overline{K} = 1$), and a continuous unzipping at higher load ($\overline{K} = 2$). At an intermediate load ($\overline{K} = 1.5$), the mid-plane undergoes some discontinuous closure.

McClung (1989) investigates the closure process of mode I cracks subjected to global biaxial fatigue. His 2-D finite element analyses of a cruciform specimen predict the highest S_{op}/S_{max} values for equibiaxial loading and the lowest values for shear loading, with uniaxial loading an intermediate case. Here, S_{op} and S_{max} denote the magnitudes of remote stress at crack opening and peak load, respectively. These analyses, however, do not relate directly to the modified boundary layer K–T model discussed in this paper. The presence of extra material near the center of the cruciform specimen modelled by McClung distorts the global biaxial loading near the crack tip. Specifically, the force lines bend around the crack tip and the tip no longer experiences the simple biaxial loading envisaged in the K–T model. Nonetheless, McClung (1989) makes a key observation that changes in forward plastic zone sizes alone cannot fully explain the trends in crack growth rates.

In a later paper, McClung (1994) conducts a direct comparison of the closure behavior for three specimen geometries (with different crack length to width, a/W, ratios) through 2-D finite element analyses. McClung shows that the normalized measure of remote stress, S_{max}/σ_0, which describes successfully the closure loads in individual specimens, does not correlate the effect of different geometries on the normalized crack opening stress S_{op}/S_{max}. However, the normalized stress intensity parameter, K_{max}/K_0, where $K_0 = \sigma_0\sqrt{\pi a}$, does correlate successfully the opening stresses across the three different geometries. This observation for these 2-D cases is compatible with the 3-D scaling parameter $K_{max}/\sigma_0\sqrt{B}$ demonstrated in our earlier work (Roychowdhury and Dodds, 2003a,b). McClung (1994) notes a strong correlation at small values of K_{max}/K_0 that deteriorates with increasing K_{max}/K_0. He postulates that accounting for T-stress effects may improve the correlation quality. The present paper demonstrates that in 3-D SSY, a two parameter characterization of crack tip fields in terms of $K_{max}/\sigma_0\sqrt{B}$ and T_{max}/σ_0 correlates successfully the normalized opening load K_{op}/K_{max} across thickness, geometries and material flow properties.

Tong (2002) investigates the influence of constraint on fatigue crack growth rate by comparing test data from three different specimen geometries [C(T), SE(T) and M(T)] subjected to the same ΔK. The crack grows more rapidly with an increase in T-stress levels from negative to positive values. Tong argues that negative T-stress favours the development of increased plasticity while positive T-stress restricts yielding and promotes increased crack growth rates. McClung's (1994) analyses, however, do not reflect this monotonic behavior. He considers three specimen geometries SE(B), SE(T) and M(T). Analysis results for all three geometries are available at two a/W ratios, 0.125 and 0.3. At both these ratios, the T-stress has a negative value for all three geometries, with the magnitude largest for the M(T) specimen and smallest for the SE(B) specimen (Anderson, 1995). For $R = 0$ and at the same K_{max}, (remote) opening stresses are highest for the M(T) and lowest for SE(T). Both McClung (1994) and Tong (2002) suggest that in addition to crack tip plasticity, the T-stress may influence the closure behavior through other aspects of deformation, e.g. effect of T-stress on COD at the same K (McClung, 1994). By employing a modified boundary layer model, the present paper demonstrates the multiple roles played by T-stress in fatigue crack closure.

McClung et al. (1991) employ detailed fringe plots of cumulative plastic strains from their finite element analyses to visualize the material transfer process associated with crack closure for plane-stress and plane-strain conditions. For plane-stress conditions, material flow from the thickness direction accommodates axial stretching in the direction normal to the crack growth. Plane-strain idealizations prohibit such material flow from the thickness direction. In-plane transverse contractions in the direction parallel to crack growth then provide the "extra" material to accommodate the normal stretching. In 3-D models, the closure process involves a more complex mechanism of material transfer. The analyses conducted by McClung et al. (1991) consider only one specimen geometry, M(T), and thus do not explore the effect of variations of in-plane constraint on plastic flow. The present paper employs similar fringe plots of plastic strain to investigate the material flow process in a 3-D configuration at various levels of T-stress.

3. Modified boundary layer approach in 3-D SSY fatigue

The SSY model idealizes conditions in which a linear-elastic, plane-stress mode I field encloses the crack front plastic zone (see Fig. 1). At each location along the through-thickness crack front, and extending into the plastic zone, a complex 3-D displacement–strain–stress field exists that simplifies to the linear-elastic, mode I plane-stress field at some distance from the front comparable to the thickness B. The effects of remote loading transmitted to the crack front region through the surrounding linear-elastic material may be described by the first two terms of the Williams (1957) solution

$$\sigma_{ij} = \frac{K_{\mathrm{I}}}{\sqrt{2\pi r}} f_{ij}(\theta) + T\delta_{1i}\delta_{1j}, \tag{2}$$

where $f_{ij}(\theta)$ define the angular variations of in-plane stress components. The constant term, T, represents an in-plane tensile (or compressive) stress parallel to the direction of crack extension. The out-of-plane stresses, σ_{3j}, vanish due to the plane-stress conditions remote from the crack front. The T-stress varies linearly with K_{I} through a non-dimensional constant, denoted β, that depends on the geometry and loading (tension, bending, thermal, etc.) (Anderson, 1995):

$$T = \frac{\beta K_{\mathrm{I}}}{\sqrt{\pi a}}. \tag{3}$$

For through-cracks, this framework has a single physical dimension (thickness B) and it captures completely the effects of different geometries and loading configurations (bending, tension,...) through the scalar K_{I}–T parameters.

Nakamura and Parks (1990) investigate the elastic–plastic fields ahead of a stationary crack under monotonic loading in a thin plate using a finite element model of the 3-D SSY configuration. From the observations of their study and anticipating a non-dimensional interplay between plastic zone size, thickness, material flow properties and R-ratio under fatigue loading, Roychowdhury and Dodds (2003a,b) establish the existence of a relationship having the form

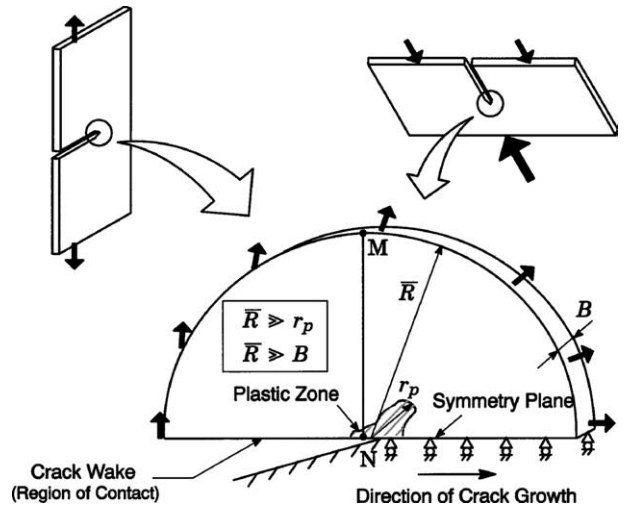

Fig. 1. 3-D mode I small-scale yielding framework for modeling fatigue crack growth. Displacements imposed on the remote boundary are those for the linear-elastic, mode I plane-stress solution with variable T-stress.

$$\frac{K_{op}}{K_{max}} = F\left(\frac{K_{max}}{\sigma_0\sqrt{B}}, \frac{z}{B}, \frac{\Delta a}{B}; R; \frac{E_T}{E}, \nu\right), \tag{4}$$

where z denotes the distance to the crack front location measured from the centerplane ($z = 0$) and E_T defines the constant tangent modulus for use in a kinematic hardening plasticity model. For simplicity, the crack front remains straight during growth (no tunneling) and a single Δa value defines the amount of crack extension. The key loading term, $K_{max}/\sigma_0\sqrt{B}$, describes essentially the maximum plastic zone sizes relative to the thickness. The non-dimensional nature of the loading term makes K_{op}/K_{max} independent of the material parameter σ_0/E, provided the ratio E_T/E remains fixed.

Our previous investigations (Roychowdhury and Dodds, 2003a,b) limit attention to configurations with β-values = 0 (no T-stress). The SE(B) specimen with $a/W \approx 0.39$, for example, represents a $\beta = 0$ geometry. The present paper broadens the scope by focusing on the effects of in-plane constraint (through T-stress) on crack closure.

Kim et al. (2001) study the stationary crack front fields in an elastic–plastic thin plate at various levels of in-plane constraint. They employ a 3-D SSY model similar to one displayed in Fig. 1 and vary the T-stress to modify the in-plane constraint level. The analyses show an expected strong influence of T-stress on crack front stresses and deformation fields. The size of the near-tip plastic zone, both at the centerplane and near the free surface, increases as the T-stress deviates from zero. A negative T-stress has a more pronounced influence on plastic deformation; the plastic zone spreads predominantly at an angle of about 45° with the forward direction of crack plane. For positive T-stress, the plastic zone tilts backward at low load ($K_{max}/\sigma_0\sqrt{B} = 1$). At a higher value of $K_{max}/\sigma_0\sqrt{B} \approx 3$, the plastic zone loses its banded appearance and spreads parallel to the crack both in the forward and the backward direction.

The above observations for a stationary crack suggest modifications of the functional relationship described by Eq. (4) in the presence of varying in-plane constraint. Anticipating that T-stress participates in a dimensionally consistent manner, we expect the new $\overline{K}$ scaling law to have the form

$$\frac{K_{op}}{K_{max}} = F\left(\frac{K_{max}}{\sigma_0\sqrt{B}}, \frac{T_{max}}{\sigma_0}, \frac{z}{B}, \frac{\Delta a}{B}; R; \frac{E_T}{E}, \nu\right), \tag{5}$$

where T_{max} represents the maximum value of T-stress (Eq. (2)) reached in the loading cycle. Eq. (5) implies that the normalized opening load K_{op}/K_{max} remains invariant across specimens and structures subjected to the same normalized load and constraint levels, characterized by the two parameters $\overline{K} = K_{max}/\sigma_0\sqrt{B}$ and $\overline{T} = T_{max}/\sigma_0$. At extended amounts of fatigue crack growth (steady state), the opening loads become constant and the dependence on $\Delta a/B$ drops out of Eqs. (4) and (5).

The effect of T_{max}/σ_0 on the opening load K_{op}/K_{max} depends on the level of $\overline{K} = K_{max}/\sigma_0\sqrt{B}$. For zero T-stress, our previous analyses (Roychowdhury and Dodds, 2003a,b) show strong 3-D effects on closure behavior at a low loading level, $\overline{K} = 1$, which causes a plastic zone size of $\sim 0.2 \times B$ at peak load. At a larger loading level, $\overline{K} = 2$ (plastic zone size $\sim 1.0 \times B$), the difference between K_{op}/K_{max} values at the centerplane and at the outside surface decreases dramatically. The present paper investigates the influence of T_{max}/σ_0 on these two different situations.

4. Numerical procedures

4.1. Finite element model

The SSY model of thickness B consists of an edge crack and a large region of material enclosing the crack front (Fig. 1). The boundary of the domain has a radius $\overline{R} = 100B$, such that the crack front plastic zone at peak load remains well-confined within a linear-elastic (plane-stress) region and has negligible

interaction with the boundary. Two-fold symmetry of the 3-D mode I configuration allows modeling of only one-quarter of the domain. A typical mesh, shown in Fig. 2, has five layers of eight-noded isoparametric brick elements through the half-thickness. Previous analyses (Roychowdhury and Dodds, 2003b) suggest satisfactory layer thicknesses of $0.25B$, $0.15B$, $0.05B$, $0.03B$ and $0.02B$, with the smallest layer located adjacent to the free surface ($z = 0.5B$). A series of small and identical elements ahead of the crack front (see Fig. 2c) permits an equal amount of crack growth simultaneously across all layers. The convergence studies (Roychowdhury and Dodds, 2003b) dictate an element size of $L_e/B = 0.01$ in the growth direction on the crack plane. The quarter-symmetric models contain typically 11,000 nodes and 9000 elements with 90 of the smallest elements defined in each layer ahead of the crack front to support growth by node release.

4.2. Loading and boundary conditions of the SSY model

Loading of the model occurs through displacements imposed on the remote cylindrical boundary by in-plane components (u, v) that follow the modified linear-elastic, plane-stress field:

$$\boldsymbol{u} = \frac{K_I}{2\mu}\sqrt{\frac{\overline{R}}{2\pi}}\hat{\boldsymbol{u}}_K(\theta) + \frac{T}{2\mu}\overline{R}\hat{\boldsymbol{u}}_T(\theta), \tag{6}$$

where $\boldsymbol{u}$ represents the displacement field at points $(\overline{R}, \theta)$ from the crack front in the cylindrical coordinate system. These displacements are imposed uniformly at each through-thickness node location. Here μ denotes the elastic shear modulus of the material. The angular functions $\hat{\boldsymbol{u}}_K$ and $\hat{\boldsymbol{u}}_T$ can be found in any

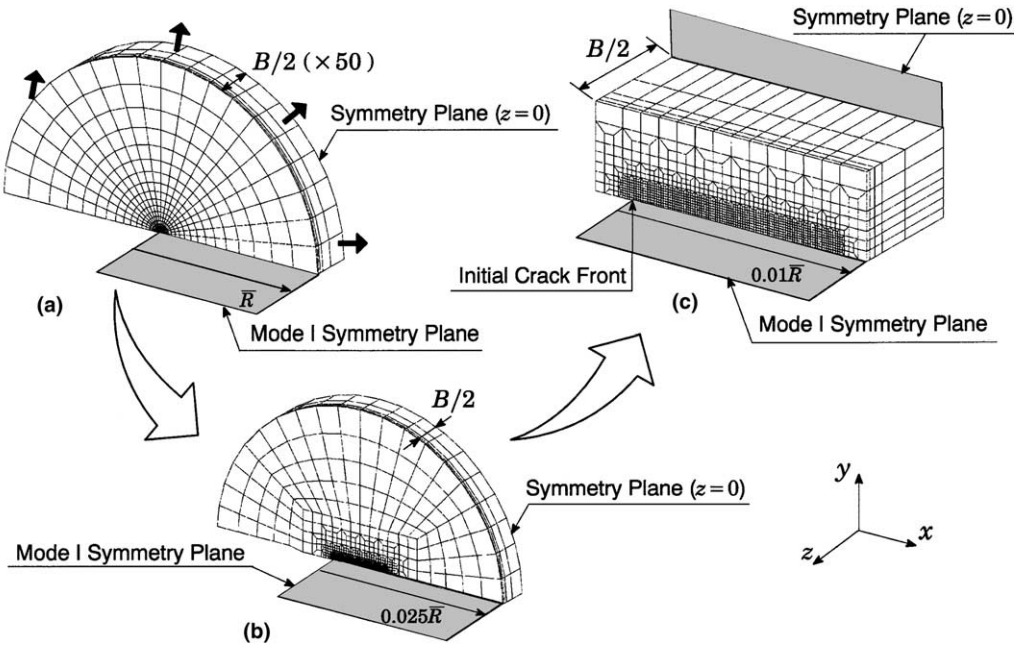

Fig. 2. Typical finite element mesh used in the 3-D small-scale yielding analyses: (a) Overall view: dimensions in thickness direction are scaled 50× for clarity; (b) transition from near-front rectangular domain to outer circular domain; (c) close-up view of the rectangular region near the crack front. The size of smallest elements ahead of the front are $L_e = 0.01B$.

fracture mechanics text book (see Anderson, 1995). Eq. (6) describes the near-tip displacement field corresponding to the stress distribution shown in Eq. (2). All nodes on the center (symmetry) plane ($z = 0$) have $w = 0$ while nodes on crack plane ($y = 0$) at, and ahead of, the current front have $v = 0$.

A load cycle consists of increasing K_I and T simultaneously from 0 to values K_{max} and T_{max}, respectively, then decreasing them back to zero. The simultaneous and proportional variations in K_I and T simulate the loading history experienced by test specimens and structures. The crack propagates uniformly over the thickness by an amount $\Delta a = L_e$ in each cycle by releasing all (current) crack front nodes in the first unloading step after the peak load. The computational procedures enforce frictionless contact conditions over the symmetry plane ($y = 0$) behind the growing crack front.

A typical load cycle employ variably sized increments specified over its duration (see Roychowdhury and Dodds, 2003a,b for details). Small increments at the start of the loading cycle ($\Delta K = 0.02K_{max}$) provide better resolution for opening load detection. The finite-sized load increments in the analysis resolve the K_{op} levels only to within the magnitude of the load increment. Small steps used after the node release point insure full redistribution of reaction forces acting on released nodes before any closing contact occurs.

4.3. Material constitutive model

The analyses use an incremental, purely-kinematic hardening constitutive model to describe the cyclic, elastic–plastic response of the material. This constitutive model shakes down fully after one cycle for both symmetric and non-symmetric loadings. The various analyses described here adopt an elastic modulus $E = 250\sigma_0$, where σ_0 denotes the initial yield stress of the material. Eq. (5) indicates that the normalized opening stress intensity factor has no functional dependence on σ_0/E (Roychowdhury and Dodds, 2003a). However, material hardening characteristics, represented through the ratio E_T/E, do influence the opening behavior. In this work, the constant hardening modulus has an assigned value of $E_T = d\sigma/d\epsilon = E/20$ for all the analyses. Poisson's ratio v has the assigned value 0.3. Our previous analyses (Roychowdhury and Dodds, 2003b) demonstrate a negligible effect of using a finite strain formulation on the K_{op}/K_{max} values. Consequently, the extensive parametric studies here adopt a small strain–displacement formulation to decrease computation runtimes.

4.4. Computational code

The finite element computations reported here are performed with the fracture mechanics research code, WARP3D (Gullerud et al., 2002). WARP3D has a software architecture that supports parallel execution via explicit message passing (MPI) coupled with shared-memory when available. The global solution procedure uses an implicit, incremental–iterative strategy with Newton iterations to achieve equilibrium at each load increment. An analysis extends the 3-D crack front once in each of 90 load cycles (the large number of cycles are needed to reach steady-growth conditions). Each load cycle requires 44 load increments with four Newton iterations generally required per increment to eliminate residual forces and to satisfy contact conditions to within a tight tolerance.

5. Results and discussion

General features of the 3-D closure process under combined K_I–T loading remain similar to those for pure mode I loading without T-stress. Specifically, near plane-strain conditions prevail in material adjacent to the centerplane ($z/B = 0$) and immediately ahead of the crack front; while material at the free surfaces ($z/B = \pm 0.5$) experiences near plane-stress conditions.

The crack opening process begins well behind the current front and progresses towards the front as K_I increases. Immediately at the front, the centerplane opens first with a smooth progression towards the free surface. Each crack front location thus has a computed value of opening stress intensity factor K_{op}. This work defines K_{op} at a crack front location when the second node behind the current crack tip loses contact with the symmetry plane upon reloading (see Roychowdhury and Dodds, 2003a,b for short discussions on this issue). A steadily rising K_{op} with crack extension marks the initial transitory phase as the crack passes through the forward plastic zone created by the first excursion to peak load. All results here correspond to a load ratio $R = K_{min}/K_{max} = T_{min}/T_{max} = 0$.

5.1. 3-D similarity scaling under K_I–T loading

Fig. 3a shows the evolution of opening load K_{op}/K_{max} with crack growth $\Delta a/B$ at different locations along the crack front computed for models with two different thicknesses, $B_1 = \underline{B}$ and $B_2 = 2 \times \underline{B}$. These two sets of results are generated with different values of the peak loads ($K^{(1)}_{max}$ and $K^{(2)}_{max}$) such that $K^{(1)}_{max}/\sigma_0\sqrt{B_1} = K^{(2)}_{max}/\sigma_0\sqrt{B_2} = 1$. In each case the models have the same normalized constraint level $T_{max}/\sigma_0 = 0.8$. Results for both cases are effectively identical. Fig. 3b shows similar results for $T_{max}/\sigma_0 = -0.8$. Analyses with other combinations of peak load ($\overline{K} = 1, 2$) and constraint level ($\overline{T} = \pm 0.4, \pm 0.8$) confirm that models with two different thicknesses subjected to same $\overline{K}$ and $\overline{T}$ loadings exhibit identical normalized opening load at all thickness layers. These results demonstrate validity of the similarity scaling, previously established under zero T-stress (Roychowdhury and Dodds, 2003a,b), for other levels of constraint. In particular, the variation of opening load K_{op}/K_{max} with crack growth $\Delta a/B$ scales with the two parameter non-dimensional load measure $K_I/\sigma_0\sqrt{B}$ and T/σ_0.

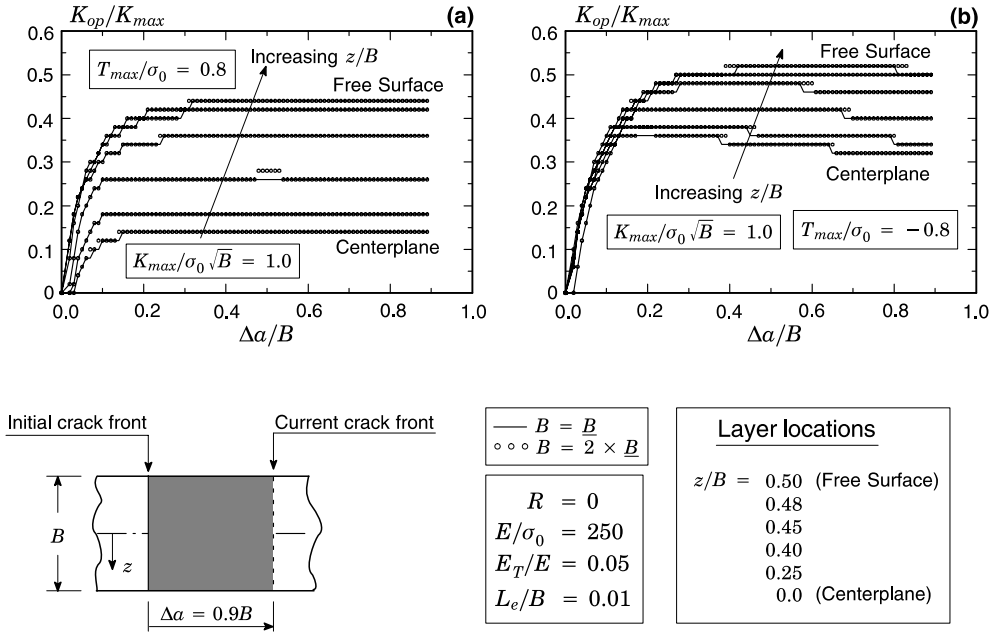

Fig. 3. Similarity scaling of normalized opening load in the presence of non-zero T-stress at each crack front location when specimens of different thickness are subject to the same normalized load (a) $\overline{K} = 1$, $\overline{T} = 0.8$; (b) $\overline{K} = 1$, $\overline{T} = -0.8$.

5.2. Effect of T-stress on opening load

Fig. 4 illustrates the effect of T-stress on crack opening at a normalized load level of $\overline{K} = K_{\max}/\sigma_0\sqrt{B} = 1$. At this peak load, the plastic zone ahead of the crack tip spreads to a distance of $\sim 0.2 \times B$ under zero T-stress (Roychowdhury and Dodds, 2003b).

The solid lines in Fig. 4a show the variation of $K_{\mathrm{op}}/K_{\max}$ with $\Delta a/B$ at different locations along the crack front for $T_{\max}/\sigma_0 = -0.4$. The broken lines pertain to constraint level $T_{\max}/\sigma_0 = 0$. At each location along the front, the curves for $T_{\max}/\sigma_0 = -0.4$ show a trend similar to $T_{\max}/\sigma_0 = 0$. Specifically, (i) the opening occurs first at the centerplane followed by a smooth transition towards the free surface; (ii) at $z/B > 0.25$, $K_{\mathrm{op}}/K_{\max}$ increases with crack extension and attains a steady value; (iii) $K_{\mathrm{op}}/K_{\max}$ at the centerplane and at midway through the thickness ($z/B = 0$ and 0.25, respectively) initially increase, then decrease when the crack grows beyond $0.2B$ and finally show a tendency to reach a steady magnitude. However, the curves at $z/B = 0$ and 0.25 for negative T-stress consistently lie above those for zero T-stress. For $T_{\max}/\sigma_0 = 0$, a large amount of crack extension ($\Delta a/B = 0.9$) decreases the magnitude of $K_{\mathrm{op}}/K_{\max}$ at the centerplane to 0.02—a value that corresponds to the resolution of the applied loading in the analysis. This suggests little or no closure at this location under zero T-stress (see also Roychowdhury and Dodds, 2003a,b). In contrast, for $T_{\max}/\sigma_0 = -0.4$ at similar amounts of crack growth, $K_{\mathrm{op}}/K_{\max}$ drops only to ~ 0.1 (and no further), indicating closure along the entire crack front. Fig. 4a also shows that at $z/B \geqslant 0.45$, the maximum difference in K_{op} for corresponding layers at $T_{\max}/\sigma_0 = 0$ and -0.4 is limited to the resolution of the applied load ($0.02K_{\max}$).

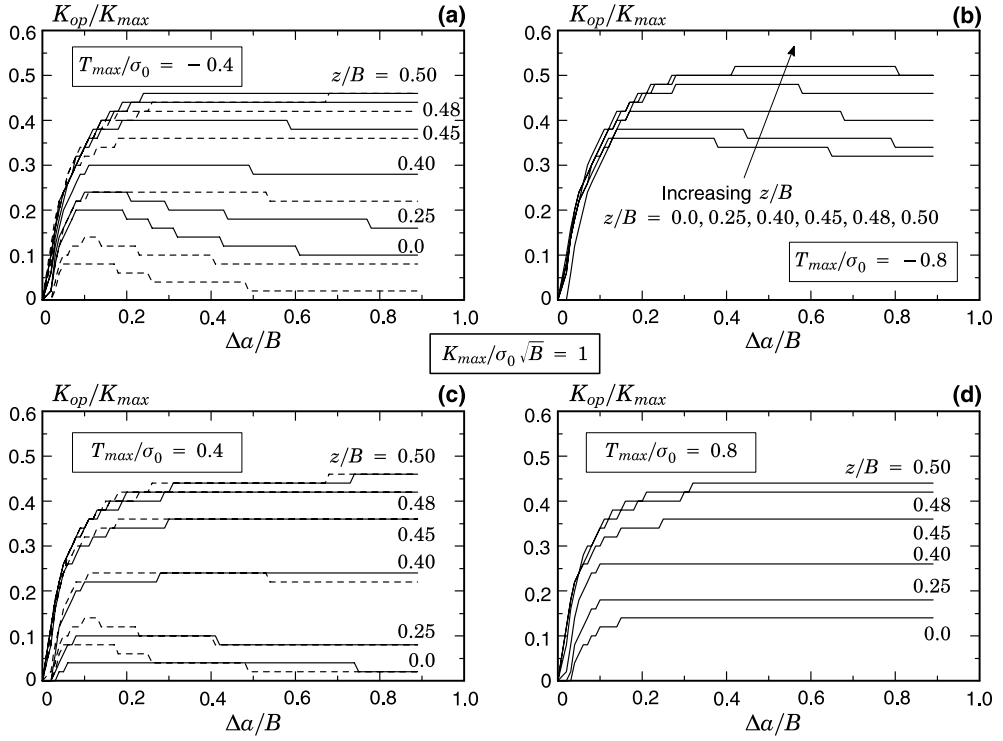

Fig. 4. Effect of T-stress on normalized opening load at $\overline{K} = 1$. The broken lines in (a) and (c) correspond to zero T-stress ($\overline{T} = T_{\max}/\sigma_0 = 0$).

The following example illustrates the significance of the results just discussed. Consider two specimens with constraint levels $T_{max}/\sigma_0 = 0$ and -0.4, both subjected to fatigue loading with peak load $\overline{K} = 1$. In a typical reloading excursion at steady state, the crack in the specimen with $T_{max}/\sigma_0 = -0.4$ remains closed at the centerplane to relatively higher loads. Opening then spreads more quickly along the front with further loading such that, near the free surface, crack opening in the two specimens occurs at similar values of K_{op}/K_{max}.

Fig. 4b shows the variation of K_{op}/K_{max} with $\Delta a/B$ at different z/B values for $T_{max}/\sigma_0 = -0.8$. A comparison of Fig. 4a and b reveals that when T_{max}/σ_0 decreases from -0.4 to -0.8, K_{op}/K_{max} values increase at all locations along the crack front. Recall from discussions in the previous paragraph, that a decrease of similar magnitude in T_{max}/σ_0 from 0 to -0.4 increases K_{op}/K_{max} only near the centerplane. The increase in K_{op}/K_{max} as T_{max}/σ_0 reduces from -0.4 to -0.8 is more pronounced near the centerplane ($z/B \leqslant 0.25$) than near the free surface ($z/B \geqslant 0.45$). For example, K_{op}/K_{max} at the centerplane increases from 0.08 to 0.32, while the free surface values change from 0.44 to 0.5. The continued closure of the crack surfaces for $T_{max}/\sigma_0 = -0.8$ relative to zero T-stress implies a smaller value of ΔK_{eff} and, consequently, a lower rate of crack growth at a given peak load $K_{max}/\sigma_0\sqrt{B} = 1.0$.

Fig. 4c and d demonstrate the effect of positive T-stress on crack closure for $\overline{K} = 1$. Fig. 4c shows that an increase in T_{max}/σ_0 from 0 (broken lines) to 0.4 (solid lines) has little effect on closure. The evolution of K_{op}/K_{max} with crack extension and its steady value remain nearly unchanged at all z/B values. When T_{max}/σ_0 increases to 0.8 (Fig. 4d), K_{op}/K_{max} shows an increase near the centerplane ($z/B \leqslant 0.25$); however, values near the free surface ($z/B \geqslant 0.45$) remain unaffected. These trends parallel those observed for $T_{max}/\sigma_0 = -0.4$. Moreover, the steady values attained by K_{op}/K_{max} at different locations along crack front are similar for $T_{max}/\sigma_0 = -0.4$ and 0.8. This also implies, at $\overline{K} = 1$, a similar decrease in crack growth rates when T_{max}/σ_0 decreases from 0 to -0.4 or increases from 0 to 0.8. Later sections show that this similarity is achieved not by a similar spread of the plastic zone in the two cases; instead it reflects a combined effect of two factors—integrated plastic strain in the crack wake and the SSY boundary displacement field at different constraint levels (Eq. (7) in Section 5.5). Unlike the case of $T_{max}/\sigma_0 = -0.4$, K_{op}/K_{max} near the centerplane exhibits no transitory decrease for the high, positive T-stress of $T_{max}/\sigma_0 = 0.8$.

Fig. 5 illustrates the effect of T-stress on crack opening at a normalized load level of $\overline{K} = 2$. At this peak load, the plastic zone ahead of the crack tip spreads to a distance of $\sim 1.0 \times B$ under zero T-stress (Roychowdhury and Dodds, 2003b). In Fig. 5a and c, the broken lines again correspond to $T_{max}/\sigma_0 = 0$. In contrast to the loading $\overline{K} = 1$, the crack now experiences substantial closure at the centerplane even at zero T-stress. Further, a comparison of the broken lines in Figs. 4a and 5a show that the difference in K_{op}/K_{max} values between the centerplane and the free surface reduces considerably when $\overline{K}$ increases from 1 to 2 (i.e., the size of the plastic zone increases from a fraction of the plate thickness to the same order of the thickness).

Fig. 5a shows that at $\overline{K} = 2$, a reduction in T_{max}/σ_0 from 0 to -0.4 has almost no effect on the evolution of crack opening load. The increase in the steady value of K_{op}/K_{max} at the centerplane for $T_{max}/\sigma_0 = -0.4$ lies within the resolution of the applied load. At other locations along the front, the steady values remain invariant of the T-stress. In sharp contrast, at $\overline{K} = 1$ a similar change in T-stress increases significantly the opening load at the centerplane and over roughly one-half of the thickness (Fig. 4a).

A reduction in the constraint level to $T_{max}/\sigma_0 = -0.8$ (Fig. 5b) impacts the opening load both at the centerplane and near the free surface. The value of K_{op}/K_{max} at $z/B = 0$ increases from 0.3 to 0.42; the corresponding increase at $z/B = 0.48$ is from 0.4 to 0.48. Further, at this constraint level the through-thickness variation in opening load K_{op} diminishes to the lowest value ($0.06K_{max}$) among all the cases considered here.

Fig. 5c compares the evolution of crack opening load for $T_{max}/\sigma_0 = 0$ and 0.4. The K_{op}/K_{max} values remain unaltered at $z/B \geqslant 0.25$ for this variation in T-stress; at $z/B = 0$, they increase slightly. By

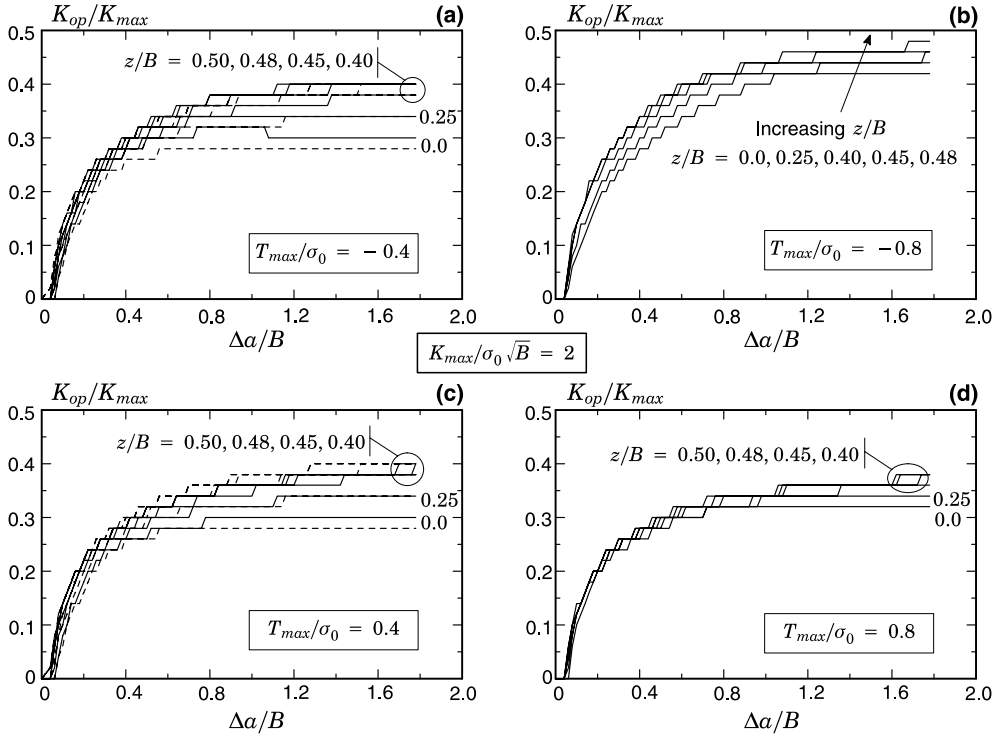

Fig. 5. Effect of T-stress on normalized opening load at $\overline{K} = 2$. The broken lines in (a) and (c) correspond to zero T-stress ($\overline{T} = T_{\max}/\sigma_0 = 0$).

comparing Fig. 5a and c, both at $\overline{K} = 2$, we see that an increase and a decrease of $T_{\max}$ by $0.4\sigma_0$ from 0 have no significant effect on crack closure behavior. Fig. 5d reveals that $T_{\max}/\sigma_0 = 0.8$ increases the steady value of $K_{\mathrm{op}}/K_{\max}$ at the centerplane and reduces it at the free surface—both by a small amount. Thus, the through-thickness variation in opening load at $T_{\max}/\sigma_0 = 0.8$ shrinks to the level observed for $T_{\max}/\sigma_0 = -0.8$. However, higher $K_{\mathrm{op}}/K_{\max}$ values at all z/B locations for the negative T-stress implies a reduced crack growth rate.

Fig. 6, generated from data shown in Figs. 4 and 5, summarizes the effect of $T_{\max}/\sigma_0$ on steady-state values of normalized opening load $(K_{\mathrm{op}}/K_{\max})_{\mathrm{ss}}$. This figure shows concisely (i) a less pronounced T-stress effect on closure at the free surface than at the centerplane; (ii) that $(K_{\mathrm{op}}/K_{\max})_{\mathrm{ss}}$ at the centerplane increases with deviations from zero T-stress and that the increase is more rapid with negative T; (iii) at all levels of T-stress, an increase in $\overline{K}$ (from 1 to 2) elevates $(K_{\mathrm{op}}/K_{\max})_{\mathrm{ss}}$ at the centerplane but the free surface values remain relatively unchanged.

Shercliff and Fleck (1990) report experiments on M(T) and SE(B) specimens to investigate the effect of specimen geometry on fatigue crack growth rates. They observe no significant influence of specimen type on crack closure. The compendium of T-stress solutions (Sherry et al., 1995) and the K_{I} solutions (Anderson, 1995) enable computation of the numerical values for $\overline{K}$ and $T_{\max}/\sigma_0$ from the material, geometry and load parameters reported by Shercliff and Fleck. In these experiments $\overline{K}$ varies over the range 0.3–0.4, while $T_{\max}/\sigma_0$ attains a value of −0.25 for the M(T) and remains near zero for the SE(B). Shercliff and Fleck report measured values of $(K_{\mathrm{op}}/K_{\max})_{\mathrm{ss}} \approx 0.25$, which lie between the values at the free surface and the centerplane shown in Fig. 6a. Extrapolation of the trend for opening load with decreasing $\overline{K}$ shown in Fig. 6 suggests that at the load of $\overline{K} = 0.4$, the centerplane experiences little or no closure. This phenomenon,

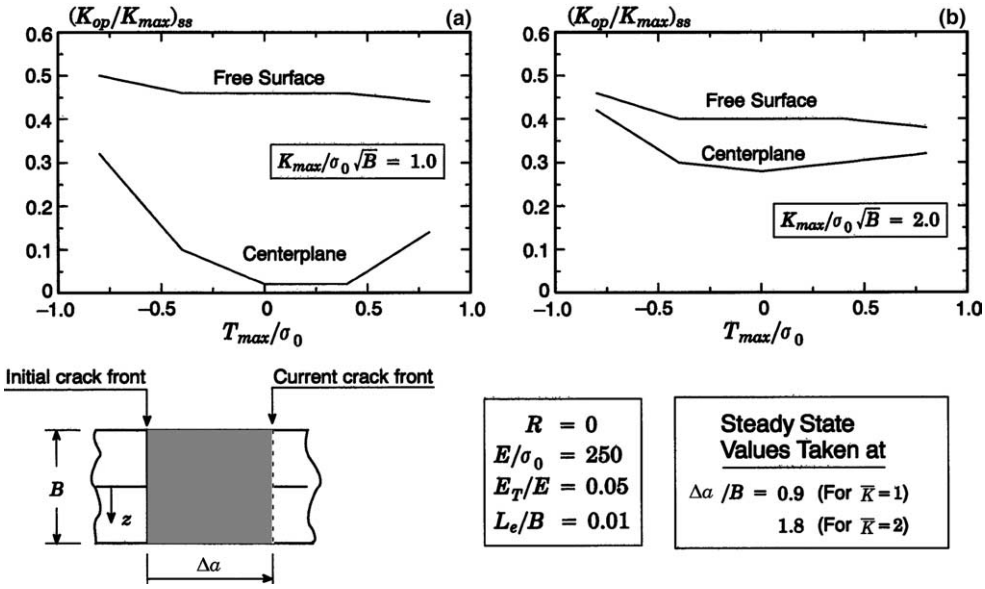

Fig. 6. Effect of T-stress on steady-state values of normalized opening load for (a) $\overline{K} = 1$, (b) $\overline{K} = 2$.

combined with the small variation in T-stress, leads to the invariance of $(K_{\mathrm{op}}/K_{\mathrm{max}})_{\mathrm{ss}}$ for these M(T) and SE(B) specimens.

In a recent study, Joyce (2004) describes carefully designed experiments in SE(B) and C(T) specimens to characterize fatigue crack growth rates of Inconel 718 both in the high cycle fatigue (HCF) and low cycle fatigue (LCF) range. The HCF test conditions correspond to a $\overline{K} = 0.4$. The normalized T-stress for the shallow-cracked SE(B), deep-cracked SE(B) and the C(T) specimens attains $T_{\mathrm{max}}/\sigma_0 = -0.08$, 0.04 and 0.09, respectively. Joyce observes no difference in crack growth rates between the specimens as predicted by Fig. 6 for such low variation in T-stress. Under LCF conditions, $\overline{K}$ reaches a value of 0.9 and the shallow-cracked SE(B) (with $T_{\mathrm{max}}/\sigma_0 = -0.16$) shows a factor of 2 lower crack growth rate than measured for the deep-cracked SE(B) (with $T_{\mathrm{max}}/\sigma_0 = 0.09$). Fig. 6a, which pertains to a similar value of $\overline{K}$, predicts higher $(K_{\mathrm{op}}/K_{\mathrm{max}})_{\mathrm{ss}}$, and correspondingly, lower crack growth rates for $T_{\mathrm{max}}/\sigma_0 = -0.16$ compared to 0.09.

5.3. Crack opening profiles

Fig. 7 displays the crack opening displacements, v, at peak load with distance from the current crack front, r, with both quantities normalized appropriately. The negative values of r indicate the location of a point behind the current crack front. Fig. 7 shows both stationary and fatigue crack profiles for $\overline{K} = 1$. The fatigue crack profiles refer to those at steady growth ($\Delta a/B = 0.69$). For stationary cracks, at all levels of T-stress, the only significant difference between the free surface and the centerplane profiles occurs over a small region adjacent to the crack front (over 1–2 elements).

The magnitude of the difference in opening displacements between the stationary and the fatigue cracks reflects the amount of residual plastic deformation (δ_{res}) left in the wake by the cyclic loading (Newman, 1976; McClung and Sehitoglu, 1989; Roychowdhury and Dodds, 2003a). Larger residuals enforce an early closure of crack surfaces during reverse loading and a late opening (higher $K_{\mathrm{op}}/K_{\mathrm{max}}$) in the reloading cycle. In contrast, a larger value of stationary crack opening displacement (COD) indicates the tendency of the crack to open early and points to a lower $K_{\mathrm{op}}/K_{\mathrm{max}}$ value. Thus, as McClung and Sehitoglu (1989) note, the

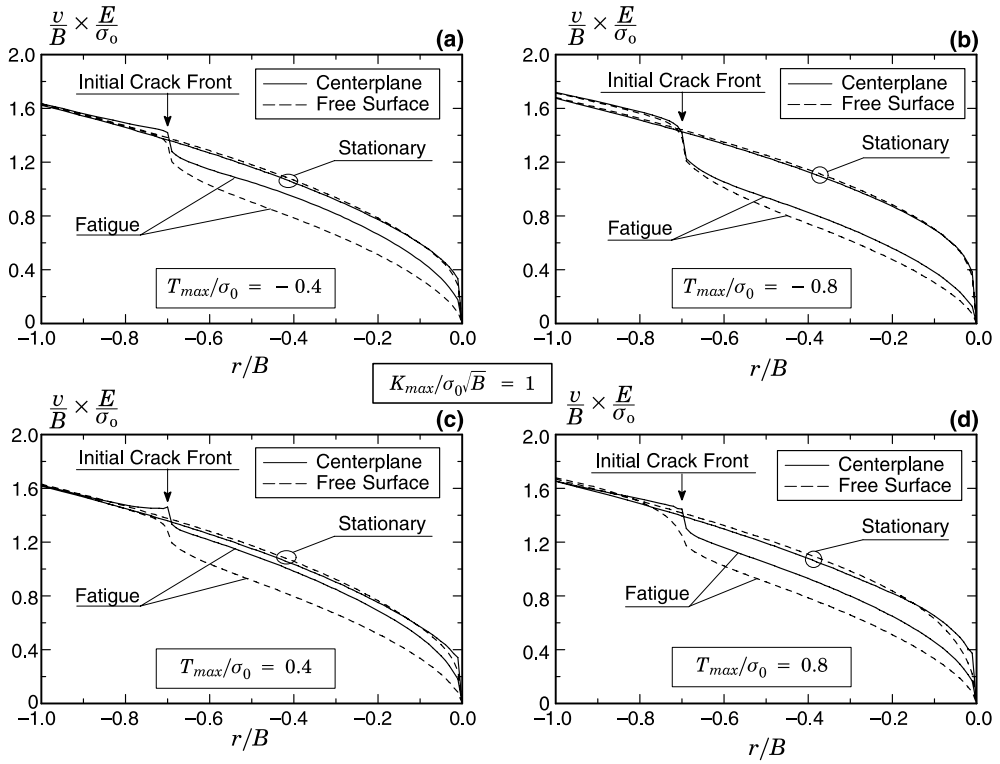

Fig. 7. Opening profiles behind the current crack front at $\overline{K} = 1$ for different levels of T-stress to illustrate the strong role of plasticity on closure behavior.

opening process can be idealized as a competition between the stationary COD and the residual displacement, δ_{res}.

Fig. 7 shows for each level of T-stress that δ_{res} at the free surface exceeds the centerplane value. In view of the insignificant difference in stationary crack CODs, the larger δ_{res} causes a higher K_{op}/K_{max} at the free surface (Fig. 4). Fig. 7a and b also reveal that the through-thickness variation in δ_{res} decreases when T_{max}/σ_0 changes from −0.4 to −0.8. This is consistent with a diminishing through-thickness variation in K_{op}/K_{max} for a similar change in T_{max}/σ_0 (Fig. 4a and b). Positive T-stress levels also exhibit similar trends in thickness variations of residual deformation and normalized opening load (Figs. 7c,d and 4c,d).

Fig. 8 illustrates the crack opening profiles at peak load for stationary and fatigue cracks at $\overline{K} = 2$. The fatigue crack profiles refer again to those at steady growth ($\Delta a/B = 1.38$). The nearly identical fatigue profiles at the free surface and at the centerplane correlate directly with the comparatively low variation in normalized opening load across the thickness at $\overline{K} = 2$ for all levels of T-stress (Fig. 5).

An analysis of the change in K_{op}/K_{max} values with T-stress must consider the effects of both the stationary COD and residual displacement, δ_{res}. At $\overline{K} = 1$, the stationary COD increases by a small amount as T_{max}/σ_0 changes from −0.4 to −0.8 (Fig. 7a and b). A larger increase in δ_{res}, particularly at the centerplane, overcomes this effect and raises K_{op}/K_{max} (Fig. 4a and b). A similar situation arises when T_{max}/σ_0 increases from 0.4 to 0.8 at $\overline{K} = 1$. Fig. 8 shows that for $\overline{K} = 2$, a change in T_{max}/σ_0, either from −0.4 to −0.8 or from 0.4 to 0.8, causes a larger increase in stationary COD values. Thus, a noticeable increase of δ_{res}, when T_{max}/σ_0 increases from 0.4 to 0.8, merely compensates for the effect of increasing COD and K_{op}/K_{max} maintains nearly the same magnitude.

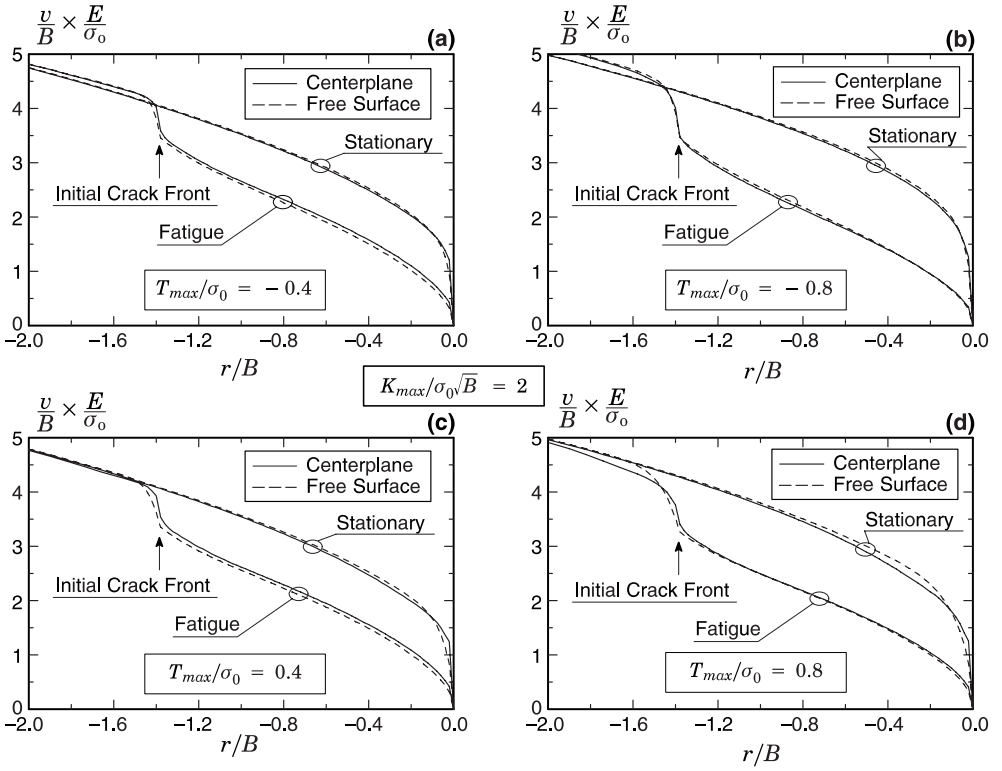

Fig. 8. Opening profiles behind the current crack front at $\overline{K} = 2$ for different levels of T-stress.

5.4. Crack opening process

Fig. 9a–c illustrate the crack opening process using a surface contact map for $K_{\max}/\sigma_0\sqrt{B} = 1$ at different levels of T-stress. The crack has grown by an amount $\Delta a/B = 0.9$ and has attained a steady-state $K_{\mathrm{op}}/K_{\max}$ value at each front location. The initial (straight) crack front located near the top of each figure has a coordinate $r/B = -0.9$. The current (straight) crack front located at the bottom of the each figure has $r/B = 0$. Left-to-right, the five images show the opening process at increasing load levels starting from $K_{\mathrm{I}}/K_{\max} = 0$ and ending at 0.4. The shaded areas indicate the closed portions of the crack surface at each stage of loading.

Fig. 9a shows that in the absence of T-stress material near the free surfaces closes fully back to the initial front location at zero load. However, the crack barely closes over half of the thickness at the center ($-0.25 \leqslant z/B \leqslant 0.25$). After a slight increase in $K_{\mathrm{I}}/K_{\max}$, only a small region near each free surface remains in contact with the symmetry plane. At $K_{\mathrm{I}}/K_{\max} = 0.4$, contact is restricted to the plane of each free surface and spreads over a very small distance ($0.04B$) behind the current crack front.

For the constraint level of $T_{\max}/\sigma_0 = -0.8$ (Fig. 9b), almost the entire crack surface closes at zero load. The early stages of reloading introduce some 3-D features as the crack opens up first near the centerplane. Further loading flattens the through-thickness opening profile. At $K_{\mathrm{I}}/K_{\max} = 0.4$, the closed region for negative T-stress reduces to a similar region for zero T-stress. Fig. 9c reveals that the evolution of crack face contact for a positive T-stress of similar magnitude lies between the responses of the zero and the negative T-stress loadings.

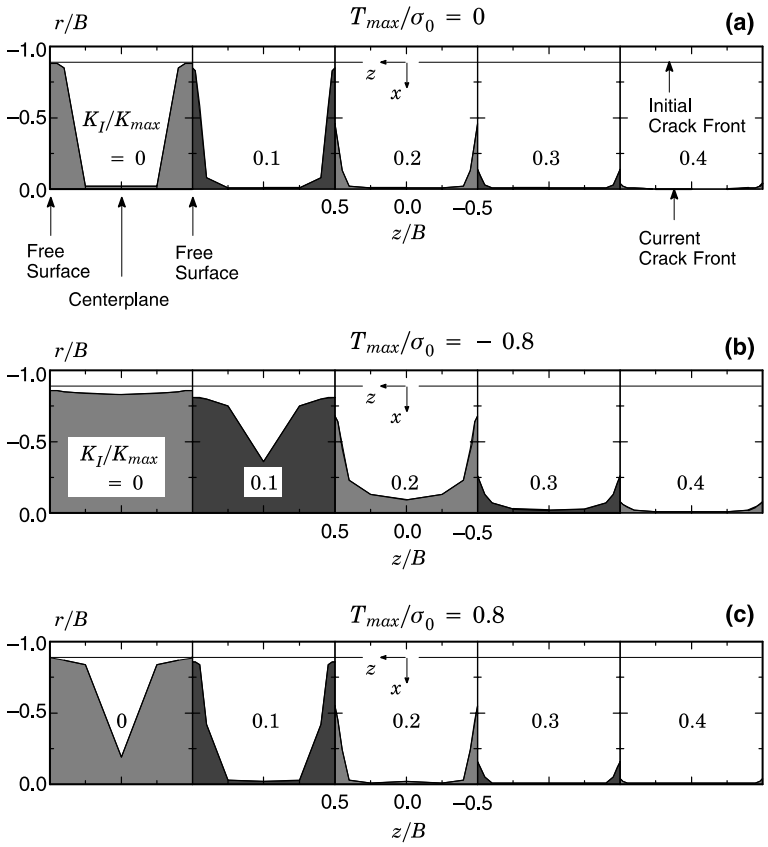

Fig. 9. Effect of T-stress on evolution of crack face contact over the symmetry plane during reloading for $\overline{K} = 1$.

Fig. 10a–c present the surface contact maps for $K_{\max}/\sigma_0\sqrt{B} = 2$. Here, the crack has grown by an amount $\Delta a/B = 1.8$. Fig. 10a shows that for this higher load level the crack face contacts the symmetry plane over a significant distance behind the current front, both at the free surfaces and at the centerplane, even for T-stress = 0. Further, at zero T-stress the opening process develops and sustains strong 3-D features (greater through-thickness variation) during the major part of reloading. A reduction in the constraint level (Fig. 10b) mitigates the through thickness variation. However, at similar values of $K_I/K_{\max}$, a larger area of the crack face remains in contact at $T_{\max}/\sigma_0 = -0.8$ compared to zero T-stress. Finally, the features of the opening process at $T_{\max}/\sigma_0 = 0.8$ (Fig. 10c) and $\overline{K} = 2$ fall between those for the zero and the negative T-stress loadings.

Figs. 9 and 10 exhibit "snapshots" of the 3-D opening process at five stages during reloading. These figures help to visualize the progression of contact loss on the crack plane. Additional quantitative results (e.g. the variation of opening load with distance behind the current crack front) confirm the following general observations. For all constraint levels, opening at any distance behind the current crack front starts at or near the centerplane and gradually spreads toward the free surface. At all thickness positions the crack face loses contact near the initial crack front location at low load. With increasing load, the crack opens in a continuous manner for both $\overline{T} = -0.8$ and 0.8.

A pattern of discontinuous crack closure emerges at and adjacent to the centerplane at $\overline{K} = 1$ and $\overline{T} = -0.4$. In this case, the layer $z/B = 0.25$ closes over a distance $\sim 0.18B$ near the current crack front and

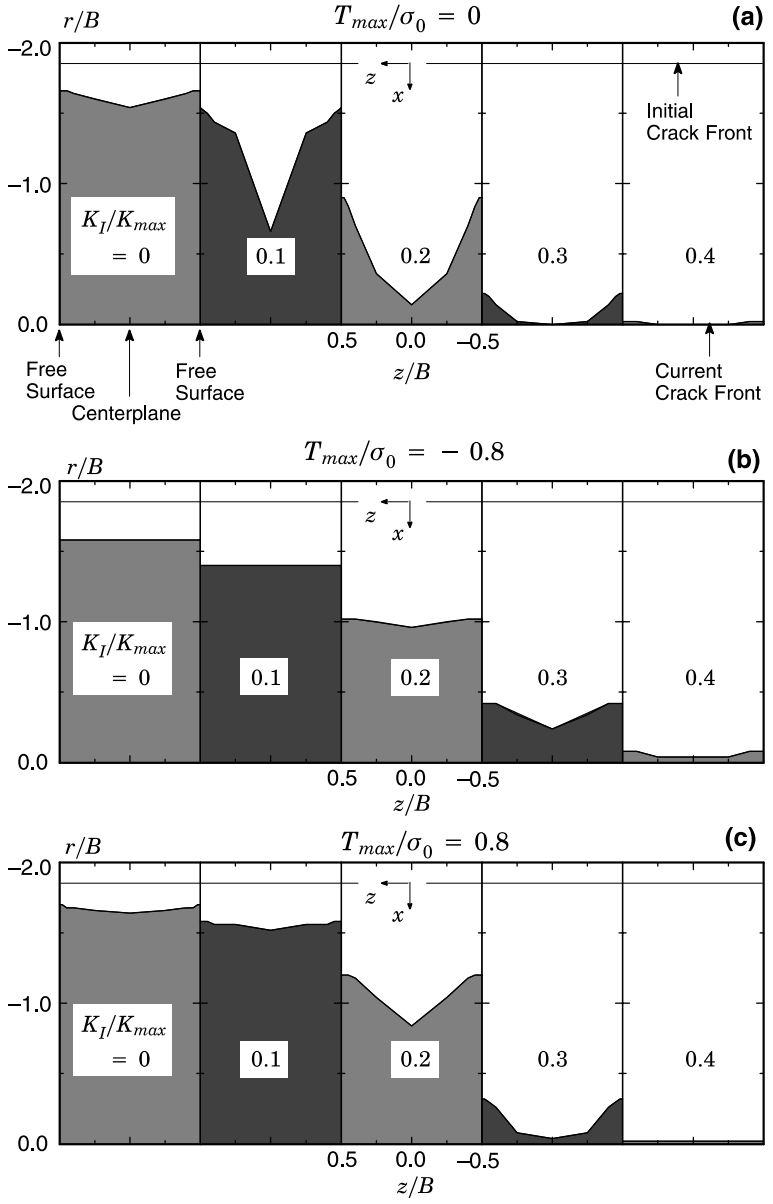

Fig. 10. Effect of T-stress on evolution of crack face contact over the symmetry plane during reloading for $\overline{K} = 2$.

over $\sim 0.15B$ near the original crack front; the nodes in between remain open even at zero load. The centerplane ($z/B = 0$) shows a similar trend with closure spread over smaller distances. The closed region near the original crack front loses contact at very early stages ($K_{op} < 0.05K_{max}$) of the next reloading cycle. Among all the cases considered here, discontinuous closure appears only for $\overline{K} = 1$ and $\overline{T} = -0.4$.

The continuous opening process occurs for $\overline{K} = 2$ at all levels of T-stress. However, the similar magnitudes of K_{op}/K_{max} at different thickness layers indicate almost instantaneous opening of the crack across thickness for the case $\overline{K} = 2$, $T_{max}/\sigma_0 = -0.8$.

5.5. Plastic flow during 3-D crack closure

The transfer of material through permanent deformation plays a key role in the mechanism of PICC. Plastic stretch in the direction normal (y) to the crack faces causes premature closure of the surfaces. The incompressibility condition of plastic deformation ($\epsilon^{pl}_{xx} + \epsilon^{pl}_{yy} + \epsilon^{pl}_{zz} = 0$) dictates that plastic contraction of either in-plane transverse (x) or thickness (z) directions (or both) must accompany stretching in the y direction. This section investigates the kinematics of 3-D plastic flow through fringe plots of plastic strain components taken at peak load.

Figs. 11–13 contain fringe plots of key plastic strain components, normalized by the yield strain ϵ_0, at peak load for $\overline{K} = 1$ corresponding to three different levels of T-stress after a crack growth of $\Delta a/B = 0.69$. In these three figures, $x/B = -0.42$ and 0.27 mark the original and the current crack front locations, respectively. Fig. 4 indicates that for this amount of crack growth, the fatigue crack has reached steady state at all constraint levels. In each of Figs. 11–13, the three plots on the left side refer to the free surface, while the right side plots refer to the centerplane. Each row corresponds to a different component of plastic strain indicated in the figures. These figures employ a consistent gray scale to facilitate direct comparisons.

Fig. 11 shows results for $\overline{K} = 1$ and zero T-stress. This figure reveals that large plastic strains spread over the length of the propagated crack and extend in the normal (y) direction to distances about one-fifth of the thickness. The positive ϵ^{pl}_{yy} fringes in Fig. 11a reflect the permanent stretch that produces crack closure. The nearly constant width of the fringes implies similar magnitudes of plastic strain over the length of the wake. Fig. 11b displays fringes for the out-of-plane, ϵ^{pl}_{zz}, component using a reverse gray scale. The fringes in

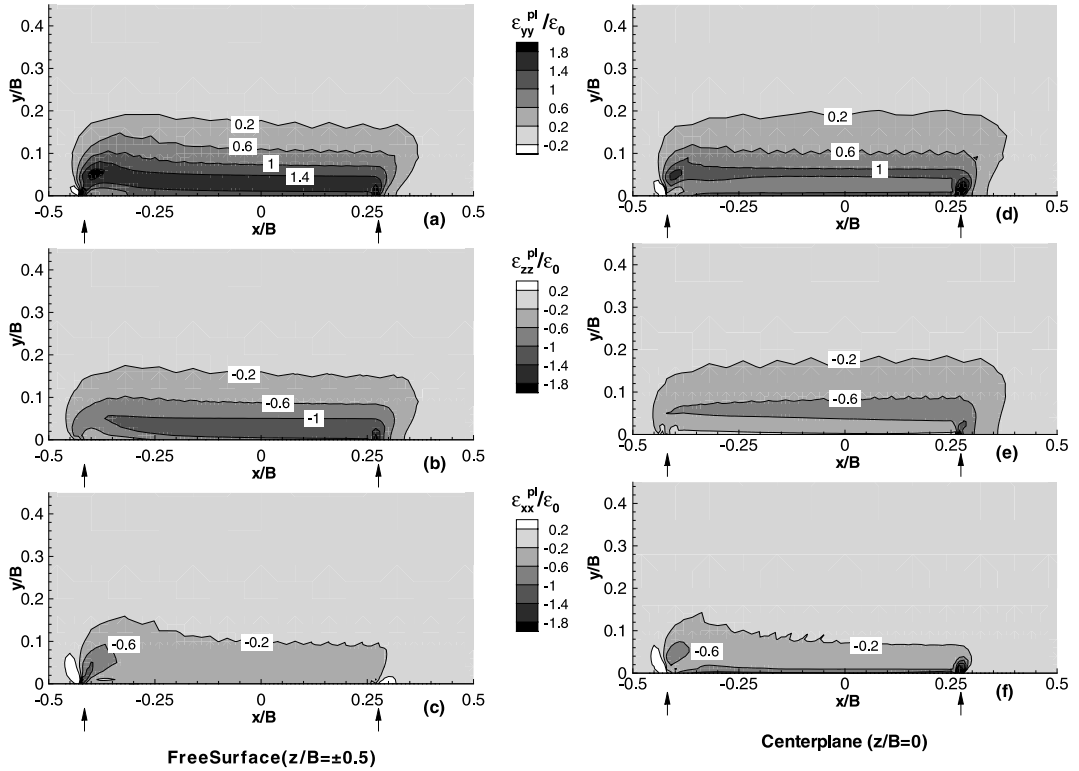

Fig. 11. Fringes of plastic strain components at peak load for $\overline{K} = 1$ and $\overline{T} = 0$. The left and right arrows indicate the locations of initial and current crack front, respectively.

Fig. 11a and b attain plastic strains of the same algebraic magnitude, but of opposite signs. The shape of the fringes in Fig. 11b are remarkably similar to those in Fig. 11a. These observations imply that a majority of the "extra" material for stretching in the normal (y) direction comes from contraction in the thickness (z) direction. The fringe with level -0.2 to -0.6 encompassing the wake in Fig. 11c indicates a smaller contribution from the in-plane transverse (x) direction.

To clarify further and to quantify the above observations, consider the point $x/B = 0, y/B = 0.04$ on the free surface. By correlating the mean value of the fringes in Fig. 11a–c, we see that this point experiences $\epsilon^{\mathrm{pl}}_{yy}/\epsilon_0 = 1.6, \epsilon^{\mathrm{pl}}_{zz}/\epsilon_0 = -1.2$ and $\epsilon^{\mathrm{pl}}_{xx}/\epsilon_0 = -0.4$. The zero sum of the components reflect the isochoric (no dilation) characteristic of plastic deformation. The magnitudes indicate that about 75% and 25% contributions from the thickness and the transverse directions, respectively, to enable the permanent normal (y) stretchings.

Fig. 11d–f show that material flows in a similar pattern near the centerplane. However, a comparative study of the fringes indicate that near the centerplane: (1) the wake experiences slightly lower plastic strain in the y and z directions, and (2) the x direction contributes a larger fraction of the required material to enable permanent y stretching, than at the free surface. These aspects of deformation on the centerplane agree very well with the plane-strain behavior observed by McClung et al. (1991).

Fig. 12 presents results in the same format for $\overline{K} = 1$, $T_{\max}/\sigma_0 = -0.8$. The plastic strains spread to a much larger distance in the vertical (y) direction compared to zero T-stress. Further, the fringes reveal the classic "leaning forward" shape observed in stationary cracks under negative T-stress (see, for example, Du and Hancock, 1991; Kim et al., 2001). Here, as in the previous figure, $\epsilon^{\mathrm{pl}}_{zz}$ and $\epsilon^{\mathrm{pl}}_{xx}$ are shown with a reverse

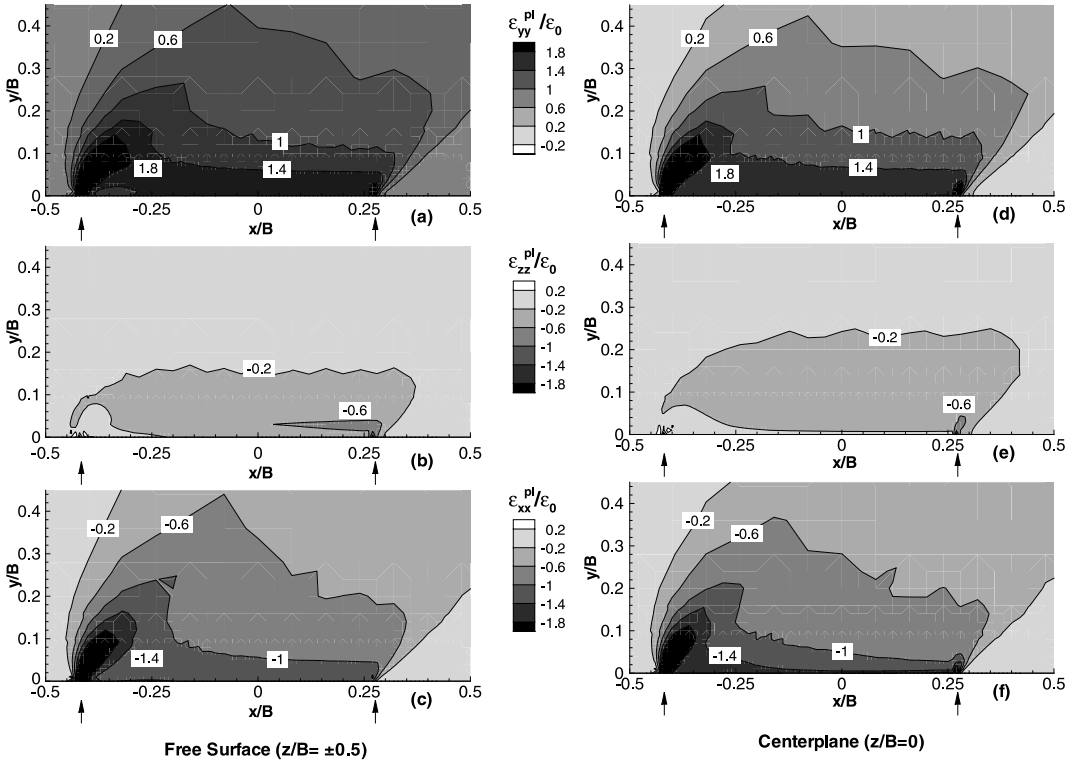

Fig. 12. Fringes of plastic strain components at peak load for $\overline{K} = 1$ and $\overline{T} = -0.8$. The left and right arrows indicate the locations of initial and current crack front, respectively.

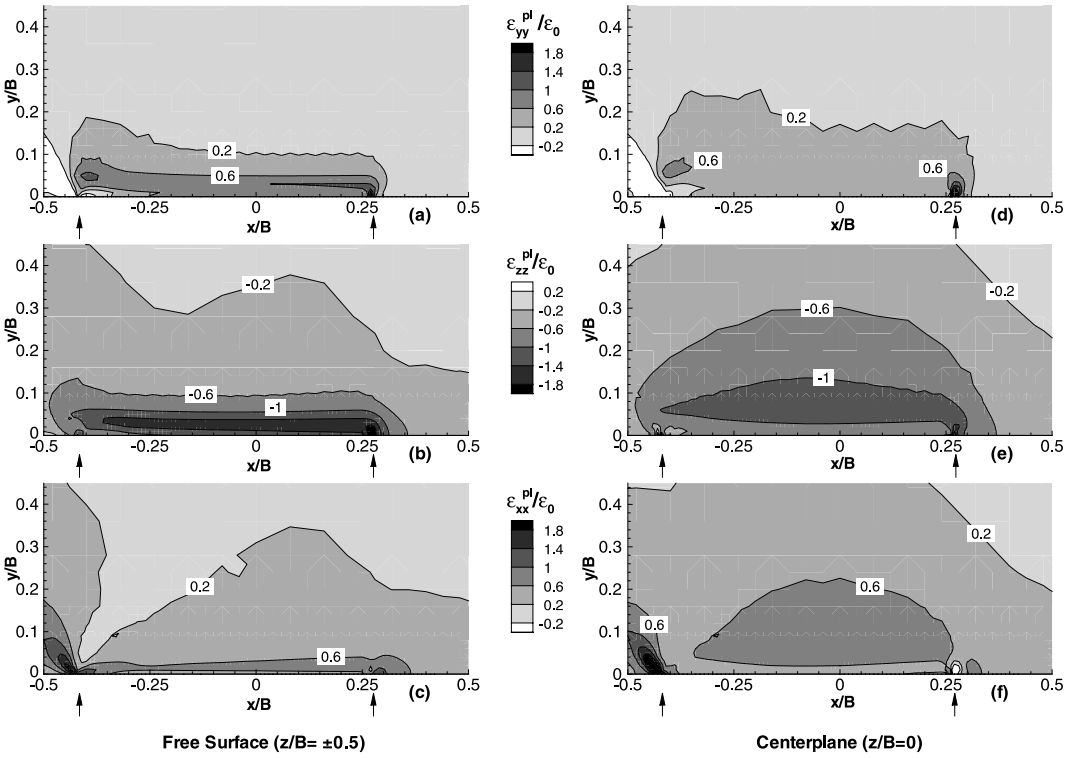

Fig. 13. Fringes of plastic strain components at peak load for $\overline{K} = 1$ and $\overline{T} = 0.8$. The left and right arrows indicate the locations of initial and current crack front, respectively.

gray scale. The y and the x components in Fig. 12 exhibit near mirror images. Thus, for the negative T-stress, the plastic contraction in the x direction transfers material to support the large y stretching, both at the free surface and at the centerplane. A quantitative analysis following the procedure described earlier asserts that at the point $x/B = 0$, $y/B = 0.04$, the in-plane transverse (x) direction contributes nearly 75% of the "extra" material in the y direction. Recall that at zero T-stress contraction in thickness (z) direction accounts for 75% of the plastic stretching in y direction. These differences demonstrate the important role played by constraint in the mechanism of plastic flow under fatigue loading. Finally, a comparison of the left and right figures shows that for negative T-stress, the centerplane and the free surface experience similar levels of plastic strain in each direction.

For $\overline{K} = 1$ and $T_{\max}/\sigma_0 = 0.8$, the crack wake experiences a much lower level of plastic deformation in the y direction (Fig. 13a and d) than for the negative and zero T-stress cases. This observation fails to explain the modest increase in opening load as T-stress changes from 0 to 0.8 (Fig. 4). Consider the line MN shown in Fig. 1. The vertical displacement (v) of the point N is given by

$$v_{\mathrm{N}} = v_{\mathrm{M}} - \int_{\mathrm{N}}^{\mathrm{M}} \epsilon_{yy}\,\mathrm{d}y. \tag{7}$$

In a typical cycle the crack faces remain closed ($v_{\mathrm{N}} = 0$) at zero load. With an increase in load, the point M moves upward for zero T-stress. A positive T-stress forces point M to move downward through the Poisson effect and keeps the crack closed to a larger load. The negative T-stress generates a larger positive magnitude of v_{M} (compared to zero T-stress), but the much higher value of the integral (through greater plastic

strains) compensates for this upward displacement. Thus, the effect of constraint on crack closure can be viewed as a competition between the first and the second term on the right hand side of Eq. (7). Figs. 7 and 8 essentially show the combined effect of these two terms as a function of distance behind the current crack front under various load and constraint levels.

Fig. 13 shows ϵ_{xx}^{pl} using the same gray scale as ϵ_{yy}^{pl}. Both these components have positive magnitude in the crack wake. Thus, for positive T-stress, contraction in the thickness direction provides the material required for permanent stretchings in both in-plane directions. At the point $x/B = 0$, $y/B = 0.02$ on the free surface, material flowing from the z direction divides equally between the x and y directions. At the centerplane, the in-plane transverse (x) direction experiences more plastic extension than the in-plane normal (y) direction.

Figs. 14–16 present the fringe plots of normalized plastic strain components at peak load for $\overline{K} = 2$ corresponding to three different levels of T-stress after a crack growth of $\Delta a/B = 1.38$. In these three plots, $x/B = -0.84$ and 0.54 mark the original and the current crack front locations, respectively. Fig. 5 indicates that for this amount of crack growth, the fatigue crack has reached steady state for all values of T-stress. The fringe levels in Figs. 14–16 reflect the much greater plastic strains attained at $\overline{K} = 2$ than at $\overline{K} = 1$.

For zero T-stress, Fig. 14 shows that the contraction in thickness direction mainly compensates for elongation in the in-plane normal direction. This effect is more pronounced at the centerplane, where ϵ_{yy}^{pl} and ϵ_{zz}^{pl} exhibit fringes of similar size and shape but opposite in sign. Contraction in the x direction contributes a small amount of material very close to the crack face ($y/B < 0.1$) on the centerplane. Interestingly, at the free surface, the x direction shares a larger fraction near the initial crack front location (see the

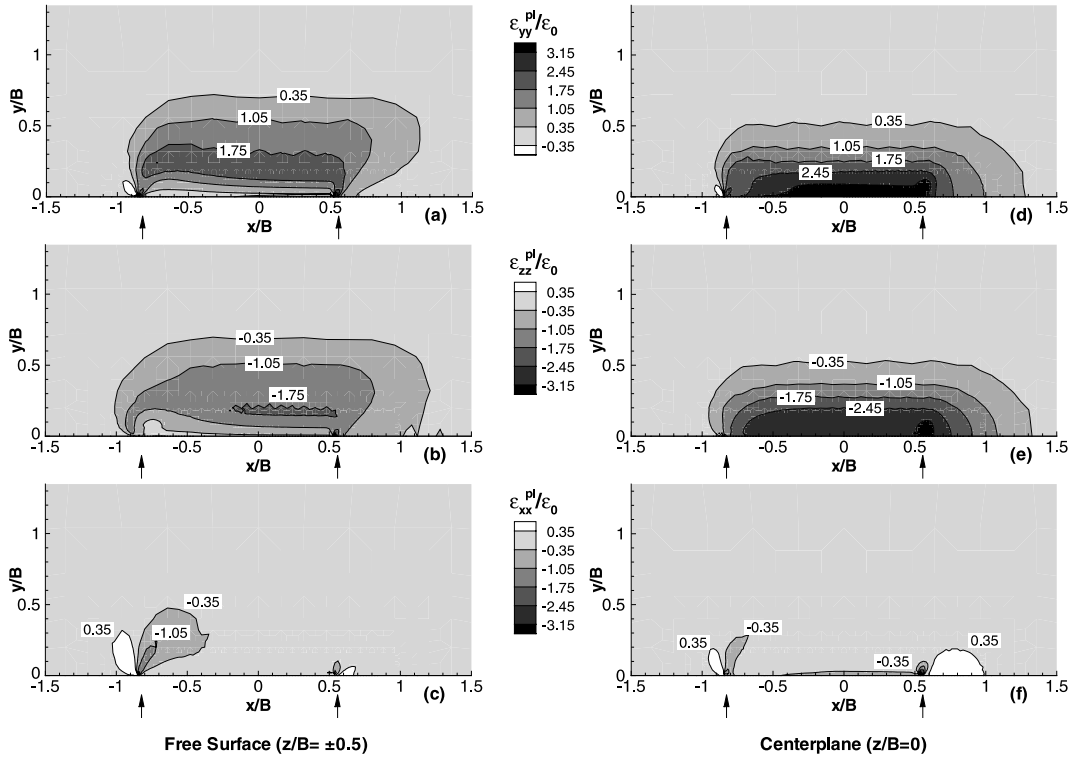

Fig. 14. Fringes of plastic strain components at peak load for $\overline{K} = 2$ and $\overline{T} = 0$. The left and right arrows indicate the locations of initial and current crack front, respectively.

concentration of fringes around the left arrow at $x/B = -0.84$ in Fig. 14c) and before the crack growth reaches a steady state.

A closer study of Figs. 11 and 14 reveals an important feature of the plastic strain distributions. At $\overline{K} = 1$, the free surface experiences larger plastic strains than the centerplane (compare Fig. 11a vs. d, or b vs. e). The situation reverses at $\overline{K} = 2$ (Fig. 14a vs. d, or b vs. e). Further, at both these load levels, the plastic zone directly ahead of the current crack front (i.e. on the symmetry plane $y/B = 0$) extends a greater distance at the centerplane than at the free surface. An observation based on the distribution of plastic strain along the crack face ($y/B = 0$) thus leads to the erroneous conclusion that at $\overline{K} = 2$ the centerplane remains closed to higher loads than the free surface. In his 2-D analyses of a cruciform specimen, McClung (1989) also finds a lack of correlation between the plastic zone size ahead of the crack and the opening load. As mentioned earlier, Eq. (7) describes closure of the crack faces. In the case of $\overline{K} = 2$, with no difference in v_M between the free surface and the centerplane (see Section 4.2), the integral on the RHS of Eq. (7) becomes the deciding factor. A larger spread of the plastic zone in the vertical direction yields a marginally higher value of the integral at the free surface, which is reflected by the crack face opening profiles (see also Roychowdhury and Dodds, 2003a).

For negative T-stress, the similar fringes with reversed signs of $\epsilon^{\mathrm{pl}}_{yy}$ and $\epsilon^{\mathrm{pl}}_{xx}$ in Fig. 15 demonstrate again that plastic compression in the x direction supplies the larger fraction of material flowing into the y direction. Following the analysis procedure outlined earlier, at the point $x/B = 0$, $y/B = 0.2$ on the free surface, the x and z directions contribute approximately 67% and 33% of the total plastic flow to the y direction. A comparison with corresponding fractions at the lower load level ($\overline{K} = 1$) with the same $T_{\max}/\sigma_0$

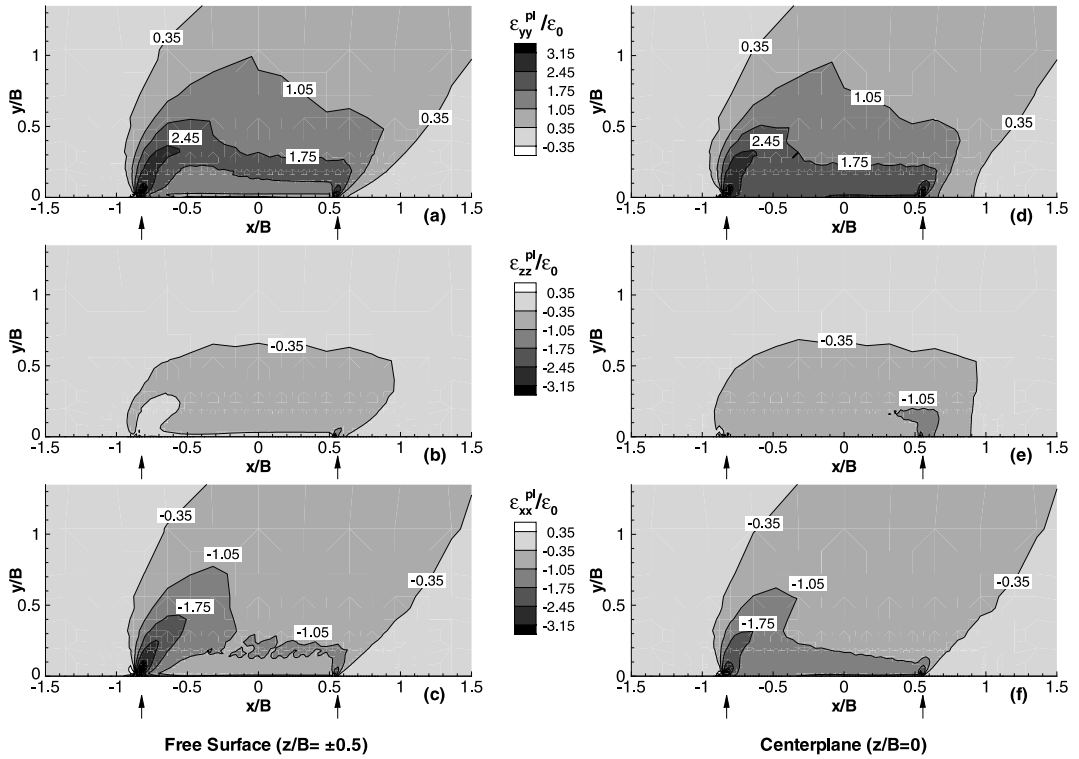

Fig. 15. Fringes of plastic strain components at peak load for $\overline{K} = 2$ and $\overline{T} = -0.8$. The left and right arrows indicate the locations of initial and current crack front, respectively.

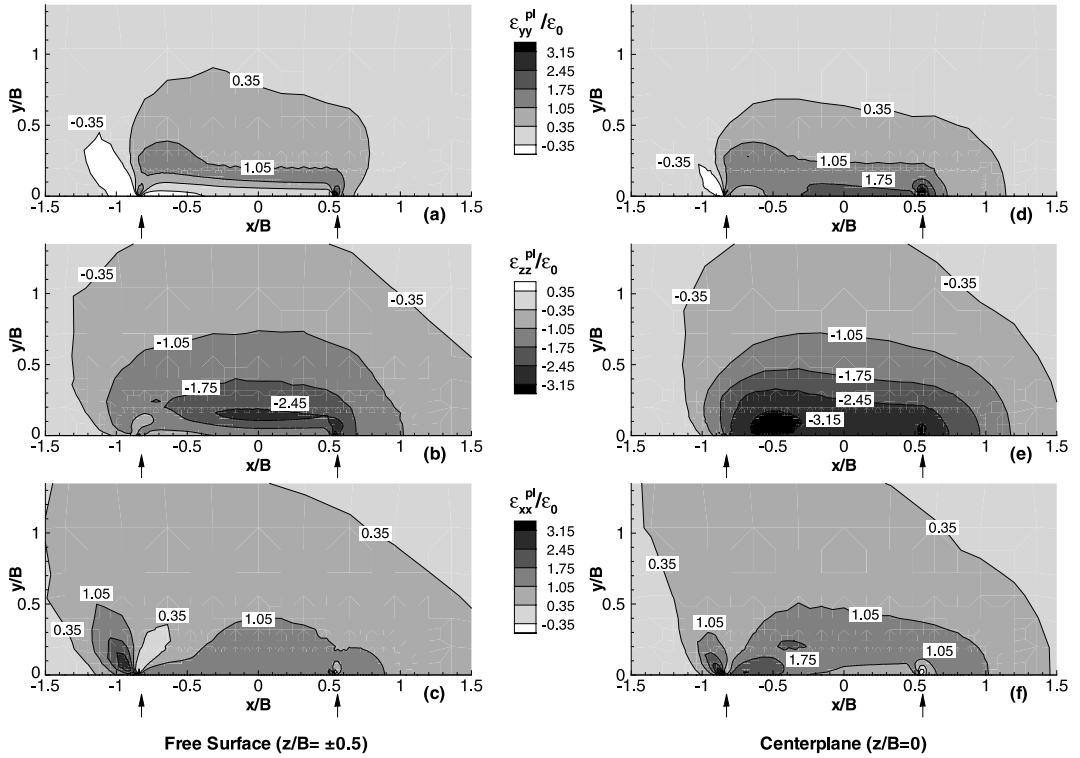

Fig. 16. Fringes of plastic strain components at peak load for $\overline{K} = 2$ and $\overline{T} = 0.8$. The left and right arrows indicate the locations of initial and current crack front, respectively.

ratio shows that the contribution from the thickness direction increases with the increase in peak load. However, away from the crack plane ($y/B > 0.7$), stretching in the y direction and shrinkage in the x direction balance each other and the thickness direction plays no significant role. Finally, the similar distributions of ϵ_{yy}^{pl} at the free surface and the centerplane (Fig. 15a and d) explain the small through-thickness variation in opening load at $\overline{K} = 2$, $T_{max}/\sigma_0 = -0.8$ (Fig. 5b).

Fig. 16 displays the plastic strain fringes for $\overline{K} = 2$, $T_{max}/\sigma_0 = 0.8$ now with only ϵ_{zz}^{pl} employing a reverse gray scale. These fringes reflect the "backward tilt" characteristic observed in stationary cracks under positive T-stress (Du and Hancock, 1991; Kim et al., 2001). The magnitudes of the different components confirm the observation that both in-plane transverse and normal directions undergo plastic extension under positive T-stress. The contraction in the thickness direction alone compensates for both these extensions.

6. Summary and Conclusions

This paper investigates the effect of in-plane constraint on 3-D fatigue crack closure in the SSY regime. The modified boundary layer model adopted here consists of a large cylindrical region of thickness B containing an edge crack and loaded remotely through a mode I, plane-stress displacement field with magnitude described by the stress intensity factor K_I and T-stress. A load cycle consists of increasing K_I and T simultaneously from zero to values K_{max} and T_{max}, respectively, and then decreasing them back to zero.

The finite element analyses extend the initially straight, through-thickness crack front by a fixed amount in each complete loading cycle using a simple node release procedure. Crack closure during reversed loading occurs when nodes behind the growing crack impinge on a frictionless, rigid plane. A bilinear, purely kinematic hardening law describes the constitutive response of the elastic–plastic material. The work presented here supports the following conclusions:

(1) Under SSY, a two parameter characterization of crack tip fields in terms of $\overline{K} = K_{\max}/\sigma_0\sqrt{B}$ and $\overline{T} = T_{\max}/\sigma_0$, where σ_0 denotes material flow stress, correlates successfully the normalized opening load $K_{\text{op}}/K_{\max}$ across variations of thickness, constraint level and material flow properties. Specifically, the evolution of $K_{\text{op}}/K_{\max}$ with normalized crack growth $\Delta a/B$, at all locations along the 3-D crack front, remains unchanged when test specimens (and/or structures) experience the same normalized load $\overline{K}$ and the same normalized constraint level $\overline{T}$.

(2) Both positive and negative deviations in T-stress from a zero value reduce the through-thickness variation of $K_{\text{op}}/K_{\max}$. This effect is more pronounced for negative T-stress and at the lower value of $\overline{K} = 1$, where the plastic zone ahead of the crack tip spreads to a distance $\sim 0.2B$ (under zero T-stress).

(3) At $\overline{K} = 1$, a small negative T-stress ($\overline{T} = -0.4$) increases $K_{\text{op}}/K_{\max}$ only at the centerplane. A large negative T-stress ($\overline{T} = -0.8$) increases $K_{\text{op}}/K_{\max}$ along the entire crack front; but the centerplane experiences a larger increase than the free surfaces. A small positive T-stress ($\overline{T} = 0.4$) has little or no effect on the opening loads. A large positive T-stress ($\overline{T} = 0.8$) increases $K_{\text{op}}/K_{\max}$ at the centerplane only.

(4) At $\overline{K} = 2$, where the plastic zone ahead of the crack tip spreads to a distance $\sim 1B$ under zero T, all levels of positive T-stress ($\overline{T} = 0.4, 0.8$) and small negative T-stress ($\overline{T} = -0.4$) have minor effect on the evolution of opening load with crack growth. The values of $K_{\text{op}}/K_{\max}$ at all locations along the crack front show a moderate increase for $\overline{T} = -0.8$.

(5) The magnitude of the T-stress influences the closure process through two factors—the stationary crack opening displacement and the residual plastic deformation left in the wake of a steadily growing fatigue crack. The opening profiles of stationary and fatigue cracks provide first order estimates of these quantities and explain qualitatively the effects of T-stress mentioned above.

(6) Crack opening at all constraint levels is essentially an ''unzipping'' process that begins at the centerplane near the initial crack front and spreads simultaneously towards the current crack front and the free surfaces. During reloading from zero in a typical cycle, negative T-stress maintains a larger fraction of the crack face area closed compared to that for zero T-stress at the same $K_{\text{I}}/K_{\max}$. The area of closure for positive T-stress lies between the zero and the negative T-stress of same algebraic magnitude.

(7) The fringe plots of individual plastic strain components reveal (a) in absence of T-stress ($T_{\max}/\sigma_0 = 0$), plastic contraction in the thickness direction compensates primarily for permanent stretching in the direction normal to crack plane required for closure; (b) for negative T-stress ($T_{\max}/\sigma_0 < 0$), plastic contraction in the in-plane transverse direction contributes the larger share of material flowing into the normal direction; (c) for positive T-stress ($T_{\max}/\sigma_0 > 0$), both in-plane directions experience permanent stretching and the thickness direction alone undergoes plastic contraction. Further, these figures show that neither the spread of plastic zone straight ahead of the crack front nor the magnitude of plastic strain on the crack face correlates directly with the variations in opening load. Deformation in the entire domain of the specimen influence the crack closure process.

Acknowledgements

The NASA-Ames Research Center and Marshall Space Flight Center provided the support for this work through Grants NAG 2-1424 (Engineering for Complex Systems Program and the NASA-Ames Chief Engineer, Dr. Tina Panontin) and NAG 8-1751 (MSFC, Mr. Doug Wells, Technical Monitor).

References

Anderson, T.L., 1995. Fracture Mechanics. CRC press, New York.

Betegon, C., Hancock, J.W., 1991. Two-parameter characterization of elastic–plastic crack-tip fields. Journal of Applied Mechanics—Transactions of the ASME 58, 104–110.

Cotterell, B., Rice, J.R., 1980. On a slightly curved or kinked crack. International Journal of Fracture 16, 155–169.

Du, Z.Z., Hancock, J.W., 1991. The effect of non-singular stresses on crack tip constraint. Journal of the Mechanics and Physics of Solids 39, 555–567.

Fleck, N.A., 1986. Finite element analysis of plasticity-induced crack closure under plane strain conditions. Engineering Fracture Mechanics 25, 441–449.

Fleck, N.A., Newman Jr., J.C., 1988. Analysis of crack closure under plane strain conditions. In: Newman Jr., J.C., Elber, W. (Eds.), Mechanics of Fatigue Crack Closure. In: ASTM STP, vol. 982. American Society for Testing and Materials, Philadelphia, pp. 319–341.

Gullerud, A.S., Koppenhoefer, K.C., Arun Roy, Y., Roychowdhury, S., Walters, M., Dodds Jr., R.H., 2002. WARP3D—Release 14.0 Manual. Civil Engineering Report No. UILU-ENG-95-2012, University of Illinois, Urbana.

Hancock, J.W., 1992. Constraint and Stress State Effects in Ductile Fracture. In: Argon, A.S. (Ed.), Topics in Fracture and Fatigue. Springer-Verlag, New York.

Hancock, J.W., Reuter, W.G., Parks, D.M., 1991. Constraint and toughness parameterized by T. In: Hackett, E.M., Schwalbe, K.-H., Dodds Jr., R.H. (Eds.), Constraint Effects in Fracture. ASTM STP, vol. 1171. American Society for Testing and Materials, Philadelphia, pp. 21–40.

Jayadevan, K.R., Narasimhan, R., Ramamurthy, T.S., Dattaguru, B., 2002. Effect of T-stress and loading rate in rate sensitive plastic materials. International Journal of Solids and Structures 39, 1757–1775.

Joyce, J.A., 2004. Evaluation of the effect of crack tip constraint on the fatigue crack growth rate of Inconel 718. In: Daniewicz, S.R., Newman, J.C., Schwalbe, K.-H. (Eds.), Fatigue and Fracture Mechanics: 34th Volume, ASTM STP 1461, ASTM international, West Conshohocken, Philadephia.

Kim, Y., Zhu, X.K., Chao, Y.J., 2001. Quantification of constraint on elastic–plastic 3D crack front by the J-A_2 three-term solution. Engineering Fracture Mechanics 68, 895–914.

Larsson, S.G., Carlsson, A.J., 1973. Influence of non-singular stress terms and specimen geometry on small-scale yielding at crack tips in elastic–plastic materials. Journal of the Mechanics and Physics of Solids 21, 263–277.

McClung, R.C., 1989. Closure and growth of mode I cracks in biaxial fatigue. Fatigue & Fracture of Engineering Materials & Structures 12, 447–460.

McClung, R.C., 1994. Finite element analysis of specimen geometry effects on fatigue crack closure. Fatigue & Fracture of Engineering Materials & Structures 17, 861–872.

McClung, R.C., 1999. Finite element analysis of fatigue crack closure: a historical and critical review. In: Proceedings of Seventh International Fatigue Conference, Beijing, China, vol. 1. pp. 495–502.

McClung, R.C., Sehitoglu, H., 1989. On the finite element analysis of fatigue crack closure-2. Numerical results. Engineering Fracture Mechanics 33, 253–272.

McClung, R.C., Thacker, B.H., Roy, S., 1991. Finite element visualization of fatigue crack closure in plane stress and plane strain. International Journal of Fracture 50, 27–49.

Nakamura, T., Parks, D.M., 1990. Three-dimensional crack front fields in a thin ductile plate. Journal of the Mechanics and Physics of Solids 38, 787–812.

Newman Jr., J.C., 1976. A finite element analysis of fatigue crack closure. In: Mechanics of Crack Growth ASTM STP, vol. 590. American Society for Testing and Materials, Philadelphia, pp. 281–301.

Rice, J.R., 1974. Limitations to the small scale yielding approximation for crack tip plasticity. Journal of the Mechanics and Physics of Solids 22, 17–26.

Roychowdhury, S., Dodds Jr., R.H., 2003a. Three-dimensional effects on fatigue crack closure in the small-scale yielding regime—a finite element study. Fatigue & Fracture of Engineering Materials & Structures 26, 663–673.

Roychowdhury, S., Dodds Jr., R.H., 2003b. A numerical investigation of 3-D small-scale yielding fatigue crack growth. Engineering Fracture Mechanics 70, 2363–2383.

Ruggieri, C., Dodds Jr., R.H., 1996. A transferability model for brittle fracture including constraint and ductile tearing effects: a probabilistic approach. International Journal of Fracture 79, 309–340.

Shercliff, H.R., Fleck, N.A., 1990. Effect of specimen geomentry on fatigue crack growth in plane strain—I. Constant amplitude response. Fatigue and Fracture of Engineering Materials and Structures 13, 287–296.

Sherry, A.H., France, C.C., Goldthorpe, M.R., 1995. Compendium of T-stress solutions for two and three dimensional cracked geometries. Fatigue & Fracture of Engineering Materials & Structures 18, 141–155.

Suresh, S., 1991. Fatigue of Materials. Cambridge University Press, Cambridge.

Tong, J., 2002. T-stress and its implication for crack growth. Engineering Fracture Mechanics 69, 1325–1337.

Williams, M.L., 1957. On the stress distribution at the base of a stationary crack. Journal of Applied Mechanics—Transactions of the ASME 24, 109–114.

Wang, Y.Y., Parks, D.M., 1992. Evaluation of the elastic *t*-stress in surface-cracked plates using the line-spring method. International Journal of Fracture 56, 25–40.

Xia, L., Shih, C.F., 1995. Ductile void growth—I. A numerical study using computational cells with microstructurally-based length scales. Journal of the Mechanics and Physics of Solids 43, 233–259.